Intense pulsed neutron generation based on the principle of Plasma Immersion Ion Implantation (PI^3) technique

By

Motloung, Setumo Victor

A thesis submitted in partial fulfilment of the requirements for the Magister Scientiae degree in the Department of Physics, University of the Western Cape.

Supervisor: Dr Chris. B. Franklyn (NECSA)

Promoter: Prof. R. Lindsay (UWC)

December 2006

Intense pulsed neutron generation based on the principle of Plasma Immersion Ion Implantation (PI^3) technique

Motloung, Setumo Victor

Keywords

Plasma Immersion Ion Implantation (PI^3) technique
Intense pulsed neutron generator
Mono-energetic neutrons
D-D and D-T reactions
Titanium target
HV pulse power supply
Plasma chamber
RF power supply
Neutron monitor and detectors
Neutron detection techniques

Abstract

Intense pulsed neutron generation based on the principle of Plasma Immersion Ion Implantation (PI^3) technique

Motloung, Setumo Victor

M.Sc thesis, Department of Physics, University of the Western Cape

The development of a deuterium-deuterium/ tritium-deuterium (D-D/ D-T) pulsed neutron generator based on the principle of the Plasma Immersion Ion Implantation (PI^3) technique is presented, in terms of investigating development of a compact system to generate an ultra short burst of mono-energetic neutrons (of order 10^{10} per second) during a short period of time (< 20μs) at repetition rates up to 1 kHz. The system will facilitate neutron detection techniques, such as neutron back-scattering, neutron radiography and time-of-flight activation analysis.

Aspects addressed in developing the system includes (a) characterizing the neutron spectra generated as a function of the target configuration/ design to ensure a sustained intense neutron flux for long periods of time, (b) the system was also characterised as a function of power supply operating conditions such as voltage, current, gas pressure and plasma density.

Declaration

I declare that *"Intense pulsed neutron generation based on the principle of Plasma Immersion Ion Implantation (PI^3) technique"* is my own work, that it has not been submitted for any degree or examination in any other university, and that all the sources I have used have been indicated and acknowledged by complete references.

Motloung Setumo Victor December 2006

Signature: .....

Acknowledgements

I would like to take this opportunity to express my gratitude to the following people and institutions:

First of all, to **OUR FATHER IN HEAVEN,** the α **and** ω for being with me all the way.

To **my parents, Thobisile Mbatha and Phutheho Motloung,** and **my family** and **friends** for their encouragement, endless love, support and for being on my side whenever I needed them.

Dr Chris. B. Franklyn, for the excellent supervision and wonderful guidance he gave me in every aspect of this research.

UWC Physics department, especially **Prof Lindsay** and the late **Dr T.K. Marais** for their critical thinking such as their contributions and their inputs for this structured masters research project.

Dr B.F. Dejene and Dr Moise Tchoule Tchokonte at UOVS (Qwaqwa), for encouraging me to take this field of physics

Mr K. Zengele, my schoolteacher, for his wonderful thoughts such as bringing the motivational days in action at my high school (Seotlong Agriculture and Hotel School).

iThemba LABS and NECSA, for their financial support and for granting me the opportunity to further up my studies with them.

Lastly, but not least I would also like to pass my gratitude to **Nolan Botha** at Necsa for his help in every aspect of this work.

Table of contents

Content	Page
Title Page	i
Keywords	ii
Abstract	iii
Declaration	iv
Acknowledgements	v
List of figures	ix
List of tables	xi
Chapter 1: Introduction	**1**
1.1 Neutron discovery	1
1.1.1 Properties and classification of neutron	2
1.1.2 Particle interaction and conservation laws	3
1.1.3 Decay of the neutron	4
1.1.4 Radiative neutron capture	5
1.2 Research background	5
1.3 The aim and study motivation	6
1.4 Thesis review/outline	7
Chapter 2: Literature Review / Theoretical Framework	**9**
2.1. Different Techniques/ Methods of neutron generation	9
2.1.1 Radioactive isotopic sources	9
2.1.2 Radioisotope (α,n) sources	10
2.1.3 Photo-neutron sources	10
2.1.4 Nuclear reaction neutron sources	11
2.1.4.1 The $^{7}Li(p,n)^{7}Be$ reaction	11

2.1.4.2 Reactions between the hydrogen isotopes 11
2.1.4.3 The $^{1}H(^{7}Li,n)^{7}Be$ reaction 12
2.1.5 Neutrons induced by particle accelerators 12
2.2 The principles of Plasma Immersion Ion Implantation (PI^3) 13
2.2.1 Basic assumptions of the PI^3 process 17
2.2.2 Negative high-voltage V_0 application to the target 18
2.2.3 Energy distributions of different times 19
2.2.4 Advantages and disadvantages of PI^3 technique 19
2.2.5 Application of Plasma Immersion Ion Implantation and Deposition (PI^3 & D) 20
2.3 Basic neutron detection 21
2.3.1 Challenges in neutron detection 21
2.3.1.1 Background noise 21
2.3.1.2 High detection-rates 22
2.3.1.3 Neutrality of neutrons 23
2.3.1.4 Multiple scattering of neutrons 23
2.3.1.5 Low and high neutron-energies 23
2.4 Types of detectors used in neutron detection 24
2.4.1 Scintillator detectors 24
2.4.2 Proportional counter detectors 25
2.5 Neutron detection techniques 28
2.5.1 Neutron back-scattering technique 29
2.5.2 Neutron Radiography (NRad) technique 30
2.5.3 Time-of-flight (TOF) technique 31

Chapter 3: Research Design and Methology **32**

3.1. The Plasma Immersion Ion Implantation (PI^3) facility at NECSA 32
3.1.1 Physical layout 33
3.1.2 Sample design/Target design 40
3.2 Sample/ target characteristics 40

3.2.1 Common ground of Plasma Immersion Ion Implantation techniques 41
3.3 Experimental setup for neutron detection 41
3.3.1 Background measurements 42
3.4 Data collection processes 44
3.5 Limitations and gaps in the data 44

Chapter 4: Results: Presentation and Discussion **45**

4.1 Description of main results 45
4.1.1 Results of neutron monitor (Bonner sphere) 45
4.1.2 Background measurements results 46
4.1.3 Predicted and calculated number of neutrons produced 48
4.1.4 Implantation of deuterium atoms into titanium target results 51
4.2 Summary of the main results and discussion of main trends 57

Chapter 5: Conclusions and Recommendations **60**

5.1 Outlook 60

Appendix A **61**

Appendix B **62**

Appendix C **64**

Appendix D **65**

References **66**

List of figures

Figure		Page
1.1	Schematic of Compton Effect.	1
1.2	Representation of Feynman diagram for the neutron decay.	4
2.1	The plot of three-dimensional relationship between energy, cross-section and angle for the D-D and D-T reactions.	16
2.2	Schematic illustration of measured detector performance (neutron counts versus detector bias-voltage).	27
2.3	Schematic presentation of neutron histories in moderated detectors.	29
2.4	Simplified layout of neutron tomography/ radiography at NECSA (NRad).	30
3.1	Schematic representation of the PI^3 technique at NECSA.	32
3.2	Schematic presentation of plasma chamber, voltage probe, current probe, deuterium gas bottle, neutron monitor and pressure meters system.	33
3.3	Schematic representation of the plasma chamber.	34
3.4	Photograph of needle valve.	35
3.5	The photos of the turbo molecular + rotary vane pump and rotary vane pump.	36
3.6	Photo of the different pressure meters value display. (a) Pressure inside the chamber display. (b) Pressure of molecular + rotary vane vacuum pump display. (c) Pressure of the gas before entering the chamber display.	37
3.7	Illustration of the differential pumping system	37
3.8	Photograph of radio frequency (rf) power	38
3.9	Photograph of the components of high voltage pulse power supply	39
3.10	Schematic diagram illustrating the electronics used for neutron detection for this experiment.	41

3.11	Schematic presentation of the connection of the NE213 liquid scintillator detector to the photomultiplier tube (PMT) and preamplifier.	42
3.12	Schematic presentation of the propagation of secondary cascade through the atmosphere [Dar01].	43
4.1	Distribution function for data given in Table 4.1	47
4.2	A diagram showing the distance between the radiation source and detector	48
4.3	Graph of number of fusion neutrons against energy for data in Table 4.7.	55
4.4	Graph of number of fusion neutrons against energy for data in Table 4.8.	55
4.5	Graph of number of fusion neutrons against energy for data in Table 4.9.	56
4.6	Graph of number of fusion neutrons against energy for data in Table 4.10.	56
4.7	Graph of number of fusion reaction occurred against energy for data in Table 4.11.	57
4.8	Photograph of the oscilloscope showing the voltage peak (a) and current peak (b) on the y-axis against time on the x-axis.	58

List of Tables

Table		Page
4.1	Background measurement results for 1000 seconds.	46
4.2	Implantation of deuterium atoms into titanium target results. All measurements were recorded at frequency of 50 Hz, with an RF voltage of 40 V and a chamber pressure of 20 mbar.	51
4.3	Implantation of deuterium atoms into titanium target results. All measurements were recorded at frequency of 50 Hz, with an RF voltage of 50 V and a chamber pressure of 18 mbar.	52
4.4	Implantation of deuterium atoms into titanium target results. All measurements were recorded at frequency of 100 Hz, with an RF voltage of 50 V and a chamber pressure of 18 mbar.	52
4.5	Implantation of deuterium atoms into titanium target results. All measurements were recorded at frequency of 200 Hz, with an RF voltage of 50 V and a chamber pressure of 18 mbar.	52
4.6	Implantation of deuterium atoms into titanium target results. All measurements were recorded at frequency of 250 Hz, with an RF voltage of 50 V and a chamber pressure of 18 mbar.	53
4.7	Optimistic and pessimistic results of implantation of deuterium atoms into titanium target, all measurements at 50 Hz and RF voltage of 40 V at chamber pressure of 20 mbar	53
4.8	Optimistic and pessimistic results of implantation of deuterium atoms into titanium target, all measurements at 50 Hz and RF voltage of 50 V at chamber pressure of 18 mbar	53
4.9	Optimistic and pessimistic results of implantation of deuterium atoms into titanium target, all measurements at 100 Hz and RF voltage of 50 V at chamber pressure of 18 mbar	54
4.10	Optimistic and pessimistic results of implantation of deuterium atoms into titanium target, all measurements at 200 Hz and RF voltage of 50 V at chamber pressure of 18 mbar	54

4.11	Optimistic and pessimistic results of implantation of deuterium atoms into titanium target, all measurements at 250 Hz and RF voltage of 50 V at chamber pressure of 18 mbar	54

CHAPTER 1

Introduction

1.1 Neutron discovery

In 1930, the German physists W. Bothe and H. Becker made a very great discovery about the neutron. They found that if the very energetic alpha particle emitted from polonium fell on light elements, such as beryllium, boron, or lithium, an unusual, very penetrating radiation was produced. At first they thought the radiation consisted of gamma radiation, although it was more penetrating than any gamma rays then known [Jef58] and the details of the experiment were very difficult to interpret on this basis.

Irene Joliot-Curie and Frederic Joliot-Curie reported the next important contribution in 1932. They found that when this unknown radiation was directed onto a paraffin target or any other hydrogenous material, it caused protons of very high energy to be ejected [htt01]. Using the analogy of the Compton Effect they then proved that the new type of radiation was not gamma radiation (see Fig 1.1 below) but must be a particle with mass. Furthermore, from the Compton Effect, they knew that photons do not have enough energy to eject protons from a paraffin target [htt01].

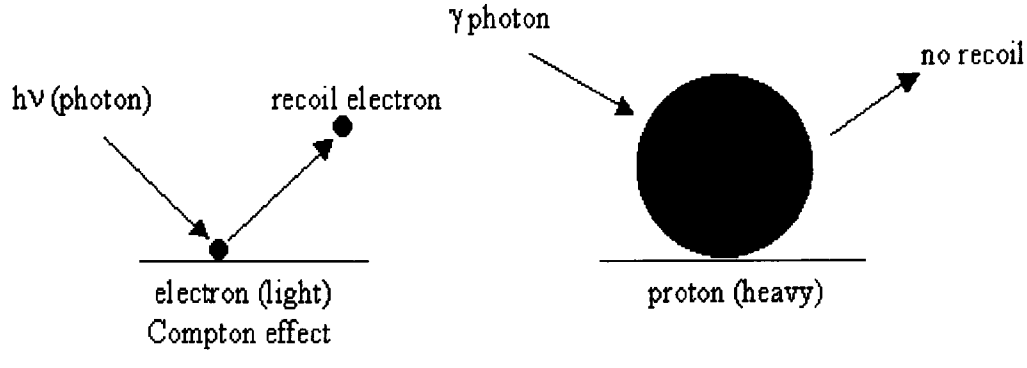

Fig 1.1. *Schematic of the Compton Effect [htt01].*

The above Fig 1.1 tries to illustrate that the electron is about 1836 times lighter than the proton and, therefore, recoil is much more pronounced for the electron than for the much heavier proton after colliding with a photon.

Finally, later in 1932 the physicist James Chadwick in England performed a series of bombardment experiments, whereby he bombarded paraffin, beryllium, helium, nitrogen and targets made of other elements using hydrogen as projectile. Comparing the energies of the recoiled charged particles from the different targets, he found that beryllium emitted a new type of radiation[1], which he suggested was comprised of uncharged particles of approximately proton mass. These new uncharged particles were called neutrons, from the Latin root for neutral [htt02, Jef58]. In conclusion, it is clear that the penetrative nature of the neutron was discovered before the neutron itself.

1.1.1 Properties and classification of neutron

The neutron is a subatomic particle with no net electric charge and mass of 939.573 MeV/c^2 (1.6749 × 10^{-27} kg slightly more than a proton, and 1839 times that of the electron). It is stable when bound in an atomic nucleus, but outside the nucleus, the neutron is unstable and has a mean lifetime of 886 seconds (about 15 minutes with an, uncertainty of about 2s). Protons and neutrons form the entire mass of atomic nuclei [htt02, htt03]. The nucleus of most atoms consists of protons and neutrons, but there is one exception in this regard, that is, the most common isotope of hydrogen (protium), which consists of a single proton only. There are two other isotopes of hydrogen;

- Deuterium (^{2}H) consisting of a proton and neutron and
- Tritium (^{3}H) consisting of a proton and two neutrons, which is unstable with a half-life of 12.3 years.

The protons and neutrons (nucleon) inside the nucleus are typically resonating between each other; by the emission and absorption of pions these nucleon particles are transformed into one another. A neutron is classified as a baryon, and consists of two down quarks and one up quark. Its

[1] A stream of particle or electromagnetic waves emitted by an atom as a result of nuclear decay or de-excitation.

spin is ½; has a magnetic moment of 1.9132 nuclear magnetons and its antiparticle is the antineutron. The De Broglie relation relates its energy and wavelength if it is moving at relativistic speeds by:

$$E = hc/\lambda \quad \ldots (1.1)$$

where E and λ are the particle energy and wavelength, respectively; h is Plank's constant $\left(6.6x10^{-34} J.s\right)$ and c is the speed of light. The particle wavelength is defined as:

$$\lambda = c/\upsilon \quad \ldots (1.2)$$

where υ is the particle frequency.

The number of neutrons in atomic nuclei determines the isotope of an element. The term isotope is defined as atoms of the same element having the same atomic number, but different masses due to the different number of neutrons [htt03]. Thus a nucleus X, is made up of Z protons and N neutrons (nucleons), with the notation ${}^{A}_{Z}X_{N}$, with atomic mass number:

$$A = Z + N \quad \ldots (1.3)$$

where X is a nuclide symbol [Map04, Kno00, Kos79].

1.1.2 Particle interaction and conservation laws

Unlike charged particles or photons, neutrons do not easily lose energy by ionizing atoms but it goes on its way until it makes a head-on collision with an atomic nucleus. For this reason, neutron radiation is extremely penetrative and very dangerous [htt02]. A neutron interacts through all four fundamental interactions, which are: the electromagnetic, weak nuclear and gravitational

interactions. Although the neutron is an uncharged particle (zero net charge), it interacts electromagnetically in two ways [htt02, htt05]:

- The neutron has a magnetic moment of the same order as the proton.
- It is composed of electrically charged quarks.

With regards to electromagnetic interaction of the neutron, it is primarily important in deep inelastic scattering and in magnetic interactions. The neutron experiences the weak interaction through beta decay[2], transforming itself into a proton, electron and antineutrino. It also experiences the gravitational force as any energetic body does, but gravitation is so weak that in most situations it may be neglected.

The most important force that neutrons experience is the strong interaction. This is responsible for the binding of the neutron's three quarks (one up quark and two down quarks) into a single particle. The strong force is also responsible for binding the nuclei (nuclear force) [htt02].

1.1.3 Decay of the neutron

The present understanding of the decay of the neutron is:

$$n \longrightarrow p + e^- + \upsilon_e^-$$

The following Feynman diagram can also present this decay process (see Fig1.2) where υ_e^- is the electron antineutrino.

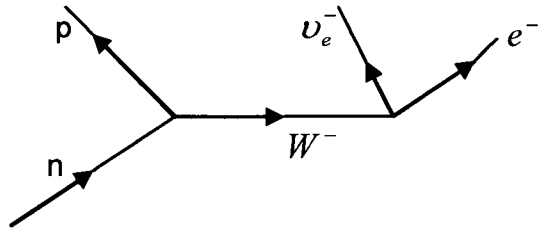

Fig 1.2. *Representation of Feynman diagram for the neutron decay [htt04].*

This decay illustrates some of the conservation laws governing particle decay. The process is mediated by a virtual W^- particle which carries away a

[2]A type of radioactive decay in which a beta particle (an e^- or e^+) is emitted. In the case of e^- emission is referred as "beta minus" (β^-), while in the case of positron as "beta plus" (β^+).

negative charge (thus charge is conserved) [htt04, htt06]. The proton in the product satisfies the conservation of baryon number, but the existence of the electron unaccompanied would violate the conservation of lepton number. The third particle must be an electron antineutrino to allow the decay to satisfy the lepton number conservation law. Furthermore spin must be conserved. The proton has spin ½ as does the electron, which adds to 0 or 1 whilst the neutron has spin ½. Thus, the $\overline{\upsilon_e}$ also has spin ½. This decay is an example of beta decay (β^-) with the emission of an electron and electron antineutrino.

1.1.4 Radiative neutron capture

This is a process whereby a substance on exposure to neutron irradiation "captures" a neutron, thus raising its mass number by one unit and giving rise to the next higher isotope of the same element. This process invariably leaves the nucleus in an "excited state"[3], and the excess energy associated with this excited state is given off in the form of electromagnetic radiation (gamma-radiation) and occasionally a charged particle or at high "capture" energies to multiple particle (neutron or proton) emission. The process is of very great importance in the production of radio-isotopes [Jef58].

1.2 Research background

Before the basic principles of plasma immersion ion implantation (PI^3) are discussed in detail, it is important to give a brief introduction to the physical background and historical development of the PI^3 technique. The fundamentals of PI^3 are traced by looking back to the work that was done in the 1960s by M. Windner and co-workers (I. Alexeff and D. Jones) [Wid70], who investigated the generation of ion acoustic waves in plasma by applying negative voltage pulses to electrode plates. The next contribution was the first PI^3 experiment performed by R. Adler and co-worker (S.T. Picraux) in the early 1980s at the Mission Research Corporation [Adl85, And02]. They developed a metal ion implanter that was based on short-pulsed vacuum arcs with synchronized negative high-voltage pulses applied to a substrate holder.

[3]State in which an atom or molecule picks up outside energy, causing an electron or nucleon to move into a higher-energy orbital

Finally and most significantly was the work reported by J.R. Conrad, R.A. Dodd, J. Frank and Worzala at the University of Wisconsin in 1986, when they realized that ion implantation by high-voltage biasing is not limited to metal ions only, but also represents an alternative way for a wide range of gas ion implantation with the potential to be a three-dimensional process [And02]. This work of Conrad and his group is generally regarded as the 'birth' of PI^3 technique.

From an application point of view, two major research directions emerged in the late 1980s and early 1990s. One was the improvement of wear and corrosion behaviour of metal surfaces, and the other research field was for large area doping of semiconductors. In general, plasma immersion ion implantation (PI^3) was developed as a tool for incorporating a three dimensionally shaped target (substrate) in the ion acceleration scheme.

But as far as this study is concerned, PI^3 is used to generate neutrons. The technology of the PI^3 process to generate neutrons began in the early 1990s. H.S. Uhm in 1991 was the first to propose using PI^3 process for neutron generation through the D-D or D-T reaction [Uhm91]. A paper was published proposing the use of PI^3 process to generate neutrons, but was never followed up. This study proposes to follow up on Uhm's proposal.

1.3 The aim and study motivation

There are many methods/techniques of generating neutrons, each with its own advantages and disadvantages, as will be presented in Chapter 2. One of the standard methods of fast neutron generation is to use the D-T reactions, creating 14.1 MeV neutrons. Such generators are commercially available but are, invariably, inefficient.

The aim of the study is to develop a compact, economical system that can deliver an intense pulse of mono-energetic neutrons based on the principles

of the PI^3 technique as it was first proposed by H.S. Uhm (see section 1.2 above). Such a neutron generator together with a combined system such as a neutron radiography set-up (see section 2.5.2) has the potential to determine the elemental composition, and not just the density of contraband materials (for example; nuclear materials, illicit drugs, money, biological materials, and explosives); due to the great penetration capability of neutrons. As far as nuclear detection methods are concerned, it is also very important to notice the advantage of such systems, as it would be difficult to shield contraband against the very probing radiation of neutrons.

The motive behind this research lies in the fact that the South African Revenue Service has recently announced that there is a requirement for scanners at South African ports and borders for the purpose of identifying contraband materials. It is this issue that makes this study so important.

1.4 Thesis review/outline

This chapter serves as an introduction to this study, which reviews the historical development of the discovery of the neutron and the PI^3 technique. This is followed by the aim and motivation of the study, which provides an outline of the problem statement. Furthermore, this thesis is organised in the following manner:

- A literature study of the aspects contained in the study forms the basis of Chapter 2. In this chapter the important key aspects such as the basic assumption that governs the PI^3 model are presented.
- Chapter 3 will discuss the experimental techniques or the setup used during the course of this study and is presented as the research design and methodology.
- The results: presentation and discussion will be presented in Chapter 4.
- Finally, conclusions and recommendations from the experimental observations are placed in Chapter 5.

Apart from these chapters, there are appendices that contain all relevant experimental data; and a bibliography follows at the end of the report.

CHAPTER 2

Literature Review / Theoretical framework

In this chapter, different techniques of neutron generation, principles of the Plasma Immersion Ion Implantation (PI^3), basic neutron detection techniques, types of detectors used for neutron detection and techniques of neutron detection are discussed.

2.1 Different Techniques/ Methods of neutron generation

Neutrons can be produced by using a number of techniques including radioactive isotopic sources, radioisotope (α,n) sources, photo-neutron sources and nuclear reactions induced by particle accelerators.

2.1.1 Radioactive isotopic sources

Isotopic neutron sources produce continuous fluxes of neutrons. One such type of source is Californium-252 (^{252}Cf). This heavy (trans-uranium) nucleus decays either by alpha emission or spontaneous fission directly emitting neutrons [www01, Cie82].

Advantages of this source are: 1) They have a usefully long life (half-life of 2.638 years, 97% of decays by α-emission, 3% by spontaneous fission) producing a relatively constant flux of neutrons on average of 3.76 neutrons per spontaneous fission; and 2) They are relatively inexpensive for low flux ($<10^8$ neutrons per second) sources. However, these sources are found to have the following disadvantages: 1) The neutron output cannot be turned off; 2) They must be contained in the bulk shielding at all times; and 3) They cannot be pulsed and the energy spectrum of the emitted neutrons is broad and peaks at energies around 1 MeV [www01].

2.1.2 Radioisotope (α,n) sources

The source of alpha particle can either be from:

- A radioisotope that decays by α-emission e.g. ^{241}Am or ^{226}Ra. Neutron emission is gained through the americium and beryllium being mixed together. The advantages of these sources are: 1) Higher specific yield of neutron sources is possible; and 2) Their availability e.g. (Am-Be are widely available) [Cie82]. Disadvantages of such sources are that: 1) Neutron output cannot be turned off; and 2) They must be contained in the bulk shielding at all times [www01]; or
- Helium ions are accelerated to high energy, using for example a Van de Graaff accelerator and then used to bombard a light target of beryllium. Production of neutrons follows the reaction below:

$$^{9}Be + ^{4}He \longrightarrow ^{12}C + n$$

The above reaction results in a higher yield of neutrons than any other target material, but this method requires relatively large physical sizes [Cie82].

2.1.3 Photo-neutron sources

Gamma-ray emitters of high energy and a suitable target material are used for the neutron production. They are based on the following photo-neutron production reactions (PNPR):

$$^{2}H + h\upsilon \longrightarrow ^{1}H + n$$

$$^{9}Be + h\upsilon \longrightarrow ^{8}Be + n$$

Advantage of these sources is that the neutron energy is mono-energetic. The disadvantage is that, in order to produce useful intensities of neutrons, high gamma-ray intensities are required [Cie82].

2.1.4 Nuclear reaction neutron sources

There are many nuclear reactions that can be used to produce neutrons. For example the neutron energy ranging between 0.1-20 MeV can be produced by the following reaction: $^{7}Li(p,n)^{7}Be$, $^{3}H(p,n)^{3}He$, $^{2}H(d,n)^{3}He$, $^{3}H(d,n)^{4}He$, $^{1}H(t,n)^{3}He$ and $^{1}H(^{7}Li,n)^{7}Be$ [Cie82]. Each and every nuclear neutron production reaction mentioned above has its advantages and disadvantages and these are discussed below.

2.1.4.1 The $^{7}Li(p,n)^{7}Be$ reaction

The reaction is widely used as a source of fast neutrons with the energies below 4 MeV. The advantage of this reaction is that; pseudo monoenergetic neutrons are only produced at proton energies between 1.92 and 2.37 MeV [Cie82]. The main problems of lithium neutron producing target are heat removal, lithium evaporation, radiation blistering, and the creation of the radioactive ^{7}Be isotope [Bay04].

2.1.4.2 Reactions between the hydrogen isotopes

The advantage of the neutron source reaction between hydrogen isotopes such as: $^{3}H(p,n)^{3}He$, **$^{2}H(d,n)^{3}He$, $^{3}H(d,n)^{4}He$** and $^{1}H(t,n)^{3}He$ is that the pseudo-monoenergetic neutron beams over the energy range of 1 to 20 MeV are produced. However, the monochromaticity of each of these sources is limited not by excited states but by thresholds for multiparticle break-up [Cie82]. The key aspect, as far as this study is concern, is that the above two underlined nuclear reactions will be considered more because they form the basis of this study, and further elaboration will be presented in section (2.2).

2.1.4.3 The $^{1}H(^{7}L,n)^{7}Be$ reaction

The main feature to emerge for a negative Q-value reaction like this is that close to threshold, the strong kinematics of the reaction confines/ focuses the emitted neutrons to a narrow cone with a high beam intensity, which simplifies shielding problems and reduces neutron background. Disadvantage of this source though, is that at higher incident energies, four line spectra are produced at zero degrees because the neutrons from the $^{1}H(^{7}Li,n)^{7}Be^{*}$ reaction are also double-valued. As a result, the use of this source requires the time-of-flight (TOF) method to select one of the neutron groups [Cie82, Dav82] and lastly, this reaction produces radioactive ^{7}Be isotopes.

2.1.5 Neutrons induced by particle accelerators

There are many types of different accelerator systems that may be used for the production of neutrons, e.g. Van de Graaff accelerator and Spallation Neutron Sources (SNS). The SNS is an accelerator based neutron source that provides the most intense pulsed neutron beams in the world as far as scientific research and industrial development [www01] are concerned. SNS are used in routine investigations of material structures using inelastic scattering and neutron diffraction. The use of SNS shows considerable benefit compared with other accelerator based neutron sources [Tec00].

The small accelerator neutron sources are useful not only for basic nuclear research and chemical analysis, but also for contraband detection such as illicit drugs, explosives and weapons [Ebe05, Tec00]. Most of them are what are generally called "sealed tube neutron generators". In the case of a small neutron research accelerator the deuterium (^{2}H) – tritium (^{3}H) reactions are the most commonly used to produce neutrons. Deuterium ions are created and accelerated into a tritium or deuterium target, producing neutrons when the deuterium atom fuses with deuterium or tritium atoms in the target via the following reactions:

$$d + t \longrightarrow n + {}^4He \qquad E_n = 14.2MeV$$

$$d + d \longrightarrow n + {}^3He \qquad E_n = 2.45MeV$$

In both cases the helium atom is created and emitted in the exact opposite directions of the neutron. Neutrons from the d-t and d-d reaction are emitted isotropically (in the centre of mass system) from the target. Estimation of the neutron flux density, n (neutrons per square cm per second), is given by:

$$n = N / 4\pi R^2 \qquad \text{... (2.1)}$$

where N is a total neutron output from neutron generator (in neutron per second), R is a distance from the deuterium or tritium target inside neutron tube to the location where neutron flux is measured. Advantages of such sources are: 1) They do not create any radiation when they are switched off; 2) They may be operated either as continuous or pulsed neutron sources; and 3) Thus produce mono-energetic neutrons [www01] e.g. 2.5 or 14 MeV plus the energy of incident ion.

2.2 The principles of Plasma Immersion Ion Implantation (PI^3)

Neutron production based on the PI^3 can also be obtained by using the deuterium-tritium and/or deuterium-deuterium reaction, whereby the deuterium ions are created and accelerated into a tritium or deuterium target and by so doing the neutrons are produced [Cie82, Ste91].

PI^3 is a technique (see Fig 3.1 and Fig 3.3) in which a target is immersed in a plasma environment of ion density of $10^9 - 10^{12}$ g. cm^{-3}, which is obtained by maintaining the pressure between 10^{-1} and 10^{-2} Pa, and the temperature of the electron generated by the applied radio frequency (rf) power in the range 2 – 10 eV. Ions within the plasma are attracted and accelerated from the plasma to the target [Ste91, Col91, Lie89]. The target is typically a palladium

rod soaked with the deuterium atoms and immersed in the plasma. The rod is connected to a high voltage module that provides a series of 1 - 10μs negative pulses with voltage ranging from 10 – 100 kV [Han91].

The negative voltage is applied to the target, in the time scale of the inverse electron plasma frequency $\omega_{pl,e}^{-1}$, which is defined by Anders [And02] as:

$$\omega_{pl,e}^{-1} = \left(\frac{\varepsilon_o m_e}{e^2 n_e} \right)^{\frac{1}{2}} \quad \ldots (2.2)$$

Where ε_0 is the permittivity of free space, n_e is the electron density, m_e and e are the electron mass and charge respectively. During this time electrons near the surface of the target are repelled and by so doing a uniform density ion matrix sheath occur [Ste91, Lie89]. The plasma sheath[4] created by the repulsion of the electrons expands dynamically according to the applied voltage, duration of the pulse and plasma density [Rky06]. During this time scale, ions are still at their original location due to their larger inertia, forming the ion matrix sheath [And02].

The deuterium or tritium atoms in the plasma become ionised because of the rf power. The distinctive features of rf power are: 1) High current density; and 2) Stable and long-life operation [Rei05].

The deuterium or tritium ions that are formed are accelerated into the palladium rod, and collide with the deuterium atoms in it. These ions impact the surface with an energy that depends on their initial position within the sheath. This results in the fusion reaction with the deuterium and tritium atoms in the target to produce neutrons [www01, Uhm91] through the following reactions;

[4]A region between a quasi-charge-neutral plasma and a physical boundary where the condition of charge neutrality no longer holds.

$$\longrightarrow \quad t(1.01MeV) + p(3.02MeV) \qquad 50\% \qquad {}^2H(d,p)^3H$$

$d + d$ D-D reaction

$$\longrightarrow \quad {}^3He(0.82MeV) + n(2.45Mev) \qquad 50\% \qquad {}^2H(d,n)^3He$$

The 50% shown in the above reaction indicates that there are equal possibilities for the reaction to produce either a proton or neutron. Although in the case of the D-T reaction there is only one branch for the reaction products and they are as follows [www01, Uhm91]:

$$t + d \longrightarrow {}^4He(3.5MeV) + n(14.5MeV) \qquad {}^2H(t,n)^4He$$ D-T reaction

The number of ions $I_{ion}\tau$ falling into the target during the pulse voltage V_0 applied increases as the applied voltage increases. The following equation derived from Uhm and Lee [Uhm91] verifies this relation.

$$I_{ion}\tau = 2.24\pi eL\left(\frac{\varepsilon_0\tau}{\sqrt{em}}V_0^{3/2}\right)^{16/29} n^{13/29} r_t^{10/29} \qquad \text{... (2.3)}$$

Where I_{ion} is the average ion current per pulse, τ is the pulse length, m is the ion mass, ε_0 is the permittivity of free space; L is the length the palladium rod, n is the plasma density and r_t is the palladium rod radius. It can also be seen from equation (2.3) that the number of ions $I_{ion}\tau$ decreases as the ion mass increases.

The approximate rate equation for the nuclear fusion to take place during the pulse, when the ions are falling into the target is described by Uhm and Lee [Uhm91] as:

$$\frac{dN}{dt} = \frac{2}{45}\sqrt{E}n_0\frac{I_{ion}}{e}\sigma(E)\Delta r \qquad \text{... (2.4)}$$

where the number density of deuterium atoms inside palladium rod is n_0, $\sigma(E)$ is the fusion cross section, E the ion kinetic energy at the target

surface, and Δr is the average penetration depth of ions into the target. For < 100 keV deuteron energies the cross section of the D-T fusion reaction is larger than that of D-D reaction (see appendix A) [Tec06]. This large cross section at a low bombarding energy has made the d-t reaction the most widely used reaction to produce highest number of neutrons [Cie82].

The graphs in Fig 2.1 show how the cross section of both reactions of interest vary as the energy and angle varies. The values presented in the graphs are given in Appendix (B-1 and B-2).

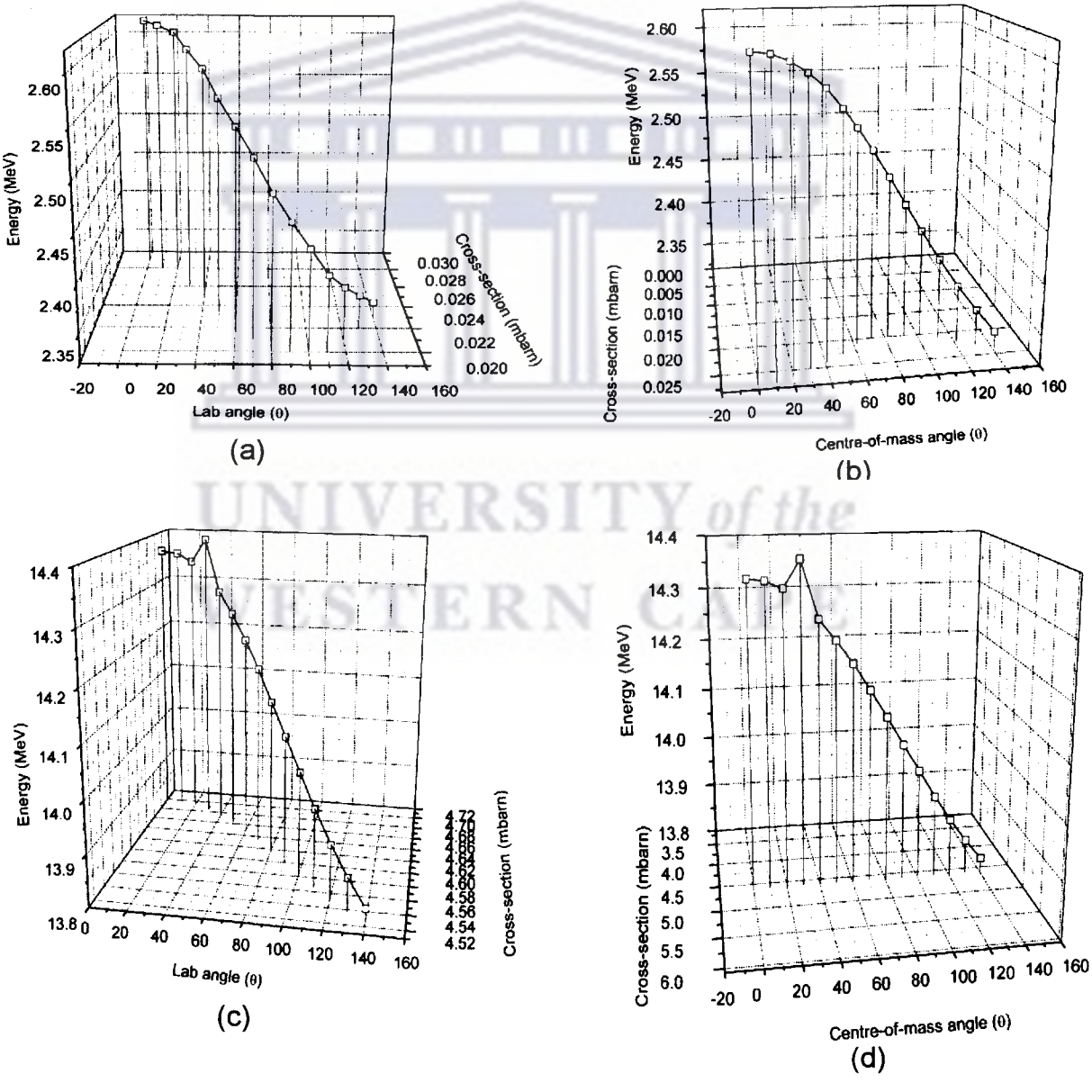

Fig 2.1. *The plot of three-dimensional relationship between energy, cross-section and angle for the D-D and D-T reactions. (a) - (b) D-D reaction (c) – (d) D-T reaction [Isb87].*

The other important facts as far as the PI^3 technique is concerned, are that the implantation of these energetic ions into the surface of the material causes sputtering because the surface of the material becomes eroded [Pro91] as a result; the atomic composition and the structure of the near region of the specific material are changed [Ste91, Lie89]. Thus, metastable phases and new materials may be generated, but it depends on the energies of the incident ions e.g. whether they are high or low. Different microstructure is produced when the implantation conditions, such as temperature and implantation energy of ions are changed and these lead to various properties. Full ion energy at the surface of the target "substrate" is obtained by keeping the pressure sufficiently low and at the same time the ion-neutral collisions in the sheath is avoided [Wol02, Sxu06]. It is these issues that form an important extension to the project with regard to selection of suitable target to contain the deuterium fusion target material.

2.2.1 Basic assumptions of the PI^3 process

The model assumptions are taken into consideration, when considering voltage pulse of amplitude V_0 with time width t_p applied to the target at time t = 0, and the plasma electrons with density n_0 repelled away from the target, resulting in the formation of an expanding non-uniform sheath. The model consists of five assumptions and is as follows:

- The ion flow is collisionless. This is valid for sufficiently low gas pressures (e.g. 0.1 Pa).
- The electron motion is inertialess. This follows because the characteristic implantation time scale much exceeds (the time scale of the inverse electron plasma frequency) $\omega_{pl,e}^{-1}$.
- The applied voltage $V \leq V_0$ is much greater than the electron temperature T_e during the entire pulse duration; hence the Debye length[5] $\lambda_D << s$ (except for $t \geq 0$) and the sheath edge are abrupt at a certain length s.
- A quasistatic Child law sheath forms [Ste91, Lie89] instantaneously at t = 0 and exists during the entire implantation. The current demanded by

[5]Is the scales over which mobile charge carriers (e.g. electrons) screen out electric field in plasma and other conductor.

this sheath is supplied entirely by the uncovering of ions at the moving sheath edge.

- During the motion of an ion across the sheath, the electric field E(x) is frozen at its initial value, independent of time, except for the change in field due to the velocity of the moving sheath [Ste91, Lie89].

2.2.2 Negative high-voltage V_0 application to the target

The applied voltage waveform is chosen to have the following form as described by Steward et al. [Ste91]:

$$\frac{V(t)}{V_0} = \begin{cases} t/t_r & 0 < t < t_r \\ 1 & t_r < t < t_r + t_p \\ (t_t - t)/t_f & t_r + t_p < t < t_p \end{cases} \quad \text{... (2.5)}$$

where $t_t = t_r + t_p + t_f$ in micro seconds. From the above voltage waveform equation it clear that the pulse is characterized by three different times: rise time t_r, plateau time t_p, and fall time t_f. The Child law current density, j_c for a voltage V_0 across a sheath thickness, s increases as the applied voltage, V_0 and ion charge, **e** increases, but when the ion mass, M and sheath thickness, s are increased the j_c is decreased. The above relationship of parameters can be verified by the following Child current equation as described by Lieberman [Lie89] as:

$$j_c = \frac{4}{9}\varepsilon_0 \left(\frac{2e}{M}\right)^{1/3} \frac{V_0^{3/2}}{s^2} \quad \text{... (2.6)}$$

where ε_0 is the permittivity of free space.

2.2.3 Energy distributions of different times

The energy distributions of different times that characterize the pulse are not the same. This means that each time e.g. rise time (t_r), plateau time (t_p) and fall time (t_f), has its own energy distribution (dN/dW). For example; energy distribution for ions entering the sheath during the pulse rise time t_r is given by [Ste91] as:

$$\left(\frac{dN}{dW}\right)_{t_r} = \left(\frac{25}{162}\right)^{1/3} \frac{n_0 s_0 t_r^{1/3}}{W^{1/6} V_0^{5/6}} \quad \ldots (2.7)$$

where n_0 is the initial ion density and W the ion implantation energy. During the voltage plateau time, t_p the ions entering the sheath receives the full energy V_0. The energy distribution is given by [Ste91] as:

$$\left(\frac{dN}{dW}\right)_{t_p} = n_0 s_0 (s_p - s_r)\delta(W - V_0) \quad \ldots (2.8)$$

where S_p is the normalized sheath position at the end of plateau time and S_r the normalized sheath position at the end of the rise time. Energy distribution during the pulse fall time t_f is given by [Ste91] as:

$$\left(\frac{dN}{dW}\right)_{t_f} = -\frac{2}{9}\frac{n_0 s_0 W^{3/2}}{V_0^{5/2}}\left[\frac{2}{3}t_p + \frac{5}{15}(t_r + t_f) - \frac{4}{15}t_f\left(\frac{W}{V_0}\right)^{5/2}\right]^{-2/3} \quad \ldots (2.9)$$

The accuracy of the model is well characterized by a single parameter, which is the ratio of the ion flight time to the pulse rise time [Ste91].

2.2.4 Advantages and disadvantages of PI^3 technique

Plasma Immersion Ion Implantation (PI^3) has several distinct advantages over the other methods of implantation, these include; uniform coverage, low unit

cost and easing line-of-sight restrictions. In this model, ions can be implanted to the concentration and depth required for surface modification. Dramatic improvements can be achieved in the life of manufacturing tools in industrial applications. The model (PI^3) is capable or has the ability to treat complex shapes [Col91], e.g. drilling rods, screws etc. The most important advantage of this model as far as this study is concerned is the fact that the PI^3 technique can produce intense pulsed neutrons.

The only disadvantage of the PI^3 technique as a neutron source is that neutrons are a form of nuclear radiation as was described in section (1.1.2). As a result, radiation protection measures should be taken into consideration when neutrons are generated through the PI^3 technique.

2.2.5 Applications of Plasma Immersion Ion Implantation and Deposition (PI^3& D)

There are many applications of the PI^3 model, although the following applications such as metallurgical and other non-semiconductor and semiconductor applications is not discussed in detail for the purpose of this thesis.

Metallurgical and other Non-Semiconductor application examples are as follows: reduction of wear and corrosion, diamond-like carbon coatings, hydrogen-free hard carbon films, deposition of other protective coatings, modification of battery electrodes, and modification of polymer surfaces.

Examples for Semiconductor applications are: flat-panel displays, silicon-on-insulator (SOI) fabrication, microcavity engineering, trench doping, and metallization technology for deep trench filling [www02].

2.3 Basic neutron detection

Neutron detection science is the effective detection of neutrons that enter a detector with a certain solid angle. Neutrons are detected in nuclear experiments by using either a neutron detector such as proportional or scintillation detectors. Multiple detectors can also be used in neutron detection experiments if a high number of neutron counts is important in the experiment. Experiments that make use of this science are scattering experiments where the scattered particles of interest are neutrons.

Two key aspects to effective neutron detection are: detection hardware and software. Detection hardware refers to the kind of detector used during the neutron detection experiment (e.g. scintillation detectors and proportional counters) and to the electronics used in the detection set-up. The hardware set-up defines the source-detector distance, detector solid angle (Ω) and shielding. While on the other hand, the detection software consists of the analysis tools that perform the task such as graphical analysis, to measure the number and energies of neutrons that strikes the detector [www02].

2.3.1 Challenges in neutron detection

Neutron detection is not an easy exercise, due to the following challenges: background noise, high detection-rate, neutrality of neutrons, multiple scattering of neutrons and practical difference in methodology of detecting low and high neutron-energies. The above-mentioned challenges affect the basic neutron detection and they are briefly explained below.

2.3.1.1 Background noise

The most prevalent problem about radiation detectors is their sensitivity to more than one type of radiation. An example is the use of the liquid scintillator NE-213 to detect neutrons, while γ-rays or cosmic rays are also present

[Zen03]. The main component in neutron detection is the background noise due to high-energy γ-rays, which are not stopped by physical barriers. Various materials such as lead, plastic and thermo-coal can easily stop other background noises such as the alphas and beta particles. Because of the above, photons are the most problematic particles in neutron detection. In addition, they also register the same energies with neutrons after scattering into the detector from the target and lastly, they are hard to distinguished from neutrons [www03].

Photons can be distinguished from neutrons by considering the slight differences in signal produced by different radiation types so that the desired type of radiation can be identified [Zen03].

2.3.1.2 High detection-rates

In charged particle and photon detectors the response time is very fast (ns) whereas for neutron detectors it is slow, since one is reliant on the neutron inducing a nuclear reaction and waiting for the secondary radiation to be detected, there is a stretched response time of up to several μs. Thus high-count rates or intense bursts of neutrons are difficult to monitor individually [Fra06] since for effective neutron detection the detector is usually placed in a region of high beam-activity, whereby it is hit by the incoming radiation (e.g. neutrons and background noise). In such a case it is not easy to understand the collected data, since the events are not easily distinguished.

In order to control high detection-rates or keeping them very low the following must be taken into consideration: 1) few events may be chosen for analysis; 2) when the events are indistinguishable from each other as stated above; the physical experimental parameters such as shielding, detector-target distance and solid angle are very important in making events distinguishable and low [www03] detection-rates can be achieved.

2.3.1.3 Neutrality of neutrons

Neutrons are electrically neutral as discussed in section (1.1.2); are only very weakly influenced by a magnetic field because of the magnetic moment of the neutron, and do not respond to an electric field. These are major problems in order to steer or accelerate them towards a detector for detection purposes [www03, Fra99]. This leads us to use methods to identify neutrons by making use of interactions taking place within a detector which generally rely on second order effects [Mcg03].

2.3.1.4 Multiple scattering of neutrons

The aspect of multiple scattering contribution is particularly important when considering the fact that; before the neutrons reaches the point of observation (detector) they usually have to travel through various layers of materials in which they can undergo interaction, but this depends on the nature of the material penetrated. These interactions can be either elastic, inelastic scatters or capture collisions [Hal38]. As a result, those that are absorbed will not be seen in the detector but those that are scattered probably will be detected. Indeed, it is difficult to devise an experiment for this purpose in which one is sure that multiple scattering and absorption are not playing a significant role [Mit35].

2.3.1.5 Low and high neutron-energies

Energies of the incoming neutrons are very important in basic neutron detection. For example in the case of low neutron-energy detection (slow neutrons i.e. energies less than 1eV) it is difficult for the detector to register/detect a measurable detection current (e.g. in scintillation detector) [www03]. This only applies to scintillation detectors because the operation of these detectors depends on the ionisation process within the detector and if the incoming neutron has very low energy the ionisation process will not occur and as a result the neutron will not be detected.

For high neutron energies (fast neutrons, typically > 100 keV) that penetrate deeply through a thick material, the neutron spectrum is usually measured by the time-of-flight (TOF) method [Sas00]. This method (TOF) is discussed in section (2.5.3) below.

2.4 Types of detectors used in neutron detection

As has been mentioned in section (2.3); the neutrons are either detected by using neutron detectors such as proportional detectors (gas filling: ^{3}He or BF_3) or scintillation detectors (^{6}Li and ZnS).

2.4.1 Scintillation detectors

The most widely used scintillation detectors include inorganic alkali halide and organic liquids. In this study the organic liquid scintillator detector NE213 is used. Inorganic scintillators have a higher efficiency in converting the radiation energy into detectable light and their response is more linear, because the generated light is proportional to the deposited energy over a wide range. The scintillation[6] mechanism in inorganic materials depends on the energy states determined by the crystal lattice of the material. The ideal scintillation material should posses the following properties [Kno00]:

- It should convert the kinetic energy of charged particle into detectable light with high scintillation efficiency.
- This conversion should be linear – the light yield should be proportional to deposited energy over a wide range as possible.
- The medium should be transparent to the wavelength of its own emission for good light collection.
- The decay time of the induced luminescence should be short so that fast signal pulses can be generated.
- The material should be of good optical quality and subject to manufacture in sizes larger enough to be of interest as practical detector.

[6]The emission of visible light when radiation is incident upon a certain material

- Its index of refraction should be near that of glass (~ 1.5) to permit efficient coupling of the scintillation light to a photomultiplier tube or light sensor.

Scintillation detectors are used in neutron detection due to the following characteristics: 1) They have excellent timing performance; and 2) They are good in pulse shape discrimination (PSD) [Jas04]. For example, a liquid scintillator gives an efficient way to discriminate between incident γ-rays and neutron by means of PSD. This method (PSD) is based on charge integration of the pulse current over two different time intervals by using charge-integration [Cer04]. The working principle of a scintillation detector used in this study (NE213 liquid scintillator) is presented in Chapter 3 section (3.2).

2.4.2 Proportional counter detectors

In this type of detector neutrons are detected through a nuclear reaction (e.g. fusion reaction), which results in energetic charged particles such as protons and alphas. The cross-section (σ) for neutron interaction in most materials is a strong function of neutron energy. Proportional counters considered in this study are based on nuclear exothermic reactions, where the gases (e.g. ^3He or BF_3) are ionised by the produced charged particle [Fra99].

The important key aspect, when searching for the nuclear reaction that might be useful in neutron detection is that, the gases of interest (e.g. ^3He and BF_3) should satisfy certain characteristics such as:

- The gas must have a high thermal cross-section, so that efficient detectors can be build with small dimensions.
- The target nucleus should have high isotopic abundance in the natural element.
- High enough Q-value for thermal reaction because the higher the Q-value, the greater will be the energy given to the reaction products and the task of discriminating against γ-ray events will be simplified by using simple amplitude discrimination.

- Gas density should allow the nearly complete stopping of the produced charged particles for enhancing the full-energy peak and reducing the wall effect [Fra99, Raw05].

Although neutrons have mass, they hold no electric charge and the methods used to recognize them are interactions within a detector and are generally relying on second order effects [Mcg03] as was mentioned in section (2.3.1.3). This means that neutron detectors must rely upon a conversion process where an incident neutron with energy E_n interacts with a target nucleus to produce a secondary charged particle, which are directly detected and the presence of neutrons can be deduced [htt05]. The most common reaction in BF_3 detector is $^{10}B(n,\alpha)^7Li$ that leads to the following products:

$$^{10}B + {}^{1}n \longrightarrow \begin{cases} {}^{7}Li(1.015MeV) + \alpha(1.777MeV) & 6\% \\ \text{Reaction Q-value} = 2.792\ \text{MeV (to ground state)} & \\ {}^{7}Li^{*}(0.840MeV) + \alpha(1.4470MeV) & 94\% \\ \text{Reaction Q-value} = 2.310\ \text{MeV (1}^{st}\ \text{excited state)} & \end{cases}$$

The decay products are released in opposite directions, when thermal neutrons (0.0259 eV) are absorbed by ^{10}B. The branching in the above reaction indicates that ^7Li may be left either in its ground (6%) or excited state (94%). From the above data it can also be realised that 94% of the reaction leaves the ^7Li ion in its first excited state, which rapidly de-excites to the ground state (~ 10^{-13}s) by the emission of a 0.480 MeV γ-rays. The remaining 6% of the reaction result in the ^7Li going directly to its ground state. The above reaction has the microscopic thermal neutron absorption cross-section of 3840 barns (1 barn = $10^{-28}m^{-2}$). In addition, this microscopic thermal neutron absorption cross-section drops rapidly with increasing neutron energy and is proportional to the inverse of the neutron velocity (1/v) over much of the energy range [Fra99, Mcg03].

On the other hand, the ^3He gas is the most suitable neutron sensitive material used as a detection medium for neutrons (e.g. LND ^3He detector). This gas is

used because of its favourable properties such as high neutron absorption cross-section and chemical inertness [Des06]. For this type of detector, the most important nuclear reaction is; $^{3}He(n,p)^{3}He$, which can be written as:

$$^{3}He + ^{1}n \longrightarrow p(0.574MeV) + ^{3}H(0.191MeV)$$ Reaction Q-value = 0.765 MeV

The thermal neutron cross-section for this reaction is 5330 barns, which is significantly higher than that for the ^{10}B reaction, and its value also depends on (1/v) [Fra99, Mcg03].

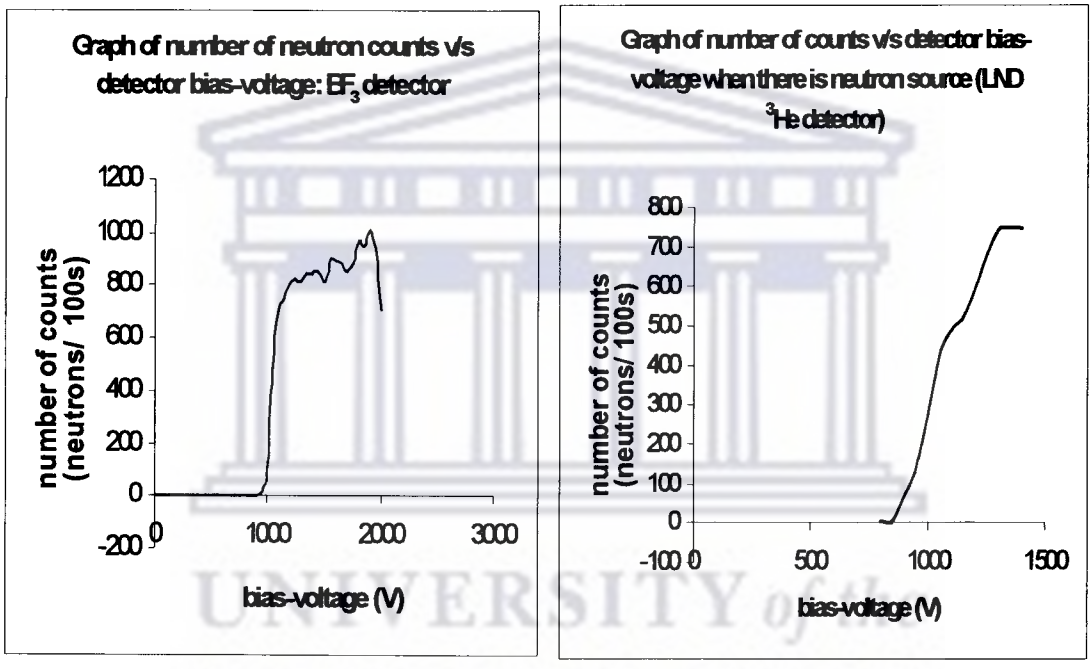

(a) (b)

Fig2.2. *Schematic illustration of measured detector performance (neutron v/s detector bias-voltage): Fig (a) BF_3 detector and (b) LND ^{3}He detector*

This leads to the comparison of ^{3}He and ^{10}B filled gas detectors, which are exactly the same in length L, radius r and solid angle (Ω). The fact that the cross-section (σ) for ^{3}He and ^{10}B differs, results in the different number of counts obtained by each detector. For example at the same bias voltage, the detectors would not have the same number of counts (see the graphs in Fig 2.2), where the LND ^{3}He is more sensitive than BF_3 detectors although they were not equal in size [Fra99]. The data for the above graphs is taken from

Appendix C. The detection efficiency for neutrons incident along the axis of a BF_3 tube is given approximately by:

$$\varepsilon(E) = \exp\left(-\sum_a (E)L\right) \quad \text{... (2.10)}$$

where $\sum_a (E)$ is macroscopic absorption cross-section of ^{10}B at energy E and L is active length of the tube Fra99]. Once one neutron has been detected, the probability of detecting another neutron that had been emitted from the source at the same time decreases exponentially with time according to the following equation:

$$p(t) = e^{\left(-t/td\right)} \quad \text{... (2.11)}$$

where p(t) equals the probability of detecting coincidence neutrons in time with td = die-away time. Where the die-away time is defined as the average time a neutron will survive before it gets absorbed in the tube (e.g. ^3He tube). The neutron die-away time normally ranges from 10-128 μs but this depends on the detector geometry. When the neutron is absorbed and the reaction products are emitted, the probability for the reaction product particles entering the detector is determined by the solid angle subtending the surface within the average effective range of the particle interaction [htt05, Fra99].

2.5 Neutron detection techniques

Neutrons can be detected with reasonable efficiency but they are virtually impossible to accelerate towards a detector for the detection purpose as was alluded in section 2.3.1.3. There are different techniques of neutron detection, this includes; neutron back-scattering, neutron radiography and the time-of-flight (TOF) technique.

2.5.1 Neutron back-scattering technique

For the general consideration, the inherently low detection efficiency for fast neutrons or any slow neutron can be improved by surrounding the detector with a few centimeters of hydrogen-containing moderating material such as the polyethylene blocks (this is shown in Fig 2.3) [Kno79]. This is important because a fast neutron can then lose a considerable fraction of its initial kinetic energy as it is back-scattered in the moderator before reaching the detector as a lower energy neutron, for which detector efficiency is generally higher.

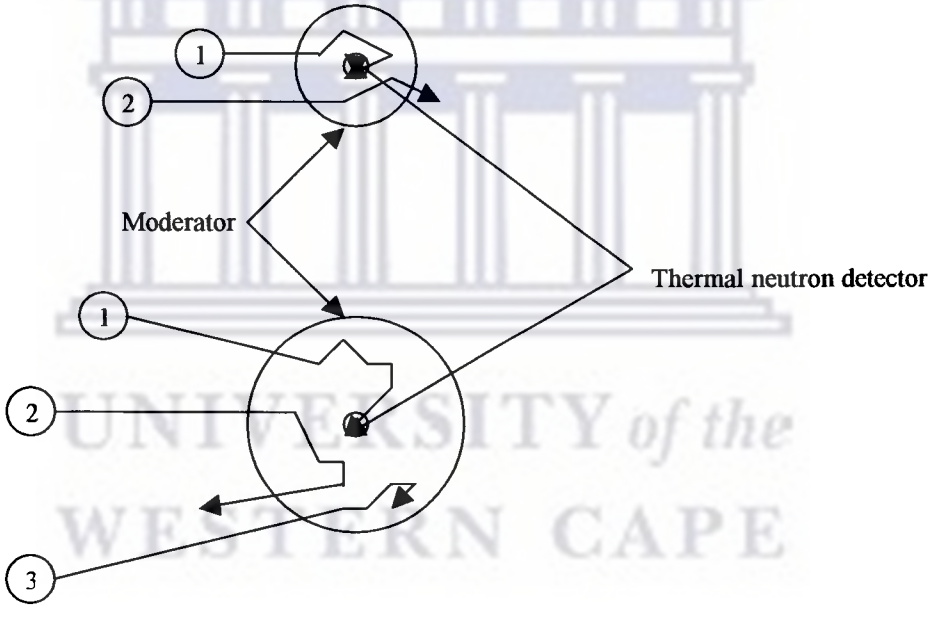

Fig 2.3. *Schematic presentation of neutron histories in moderated detectors. The small thermal neutron detector at the centre is shown surrounded by two different thicknesses of moderator material [Kno79].*

Neutrons of high energies can travel through many centimeters of matter without any type of interaction and thus can be totally invisible to a detector of common size. This is the case because the probability of most neutron-induced reactions in detectors drops off rapidly with increasing neutron energy [Kno79]. Thus, the importance of scattering becomes greater as is illustrated in Fig 2.3. From Fig 2.3, histories labeled 1 represent incident fast neutrons

that are successfully moderated and detected. Those labeled 2 are partially or fully moderated, but escape without reaching the detector. History 3 represents those neutrons that are parasitically captured by the moderator. This leads to the fact that larger moderators tend to enhance process 3 while reducing 2, as can be seen in Fig 2.3.

2.5.2 Neutron Radiography (NRad) technique

The general principle of radiography is the recording of the gamma, x-rays or neutron radiation passing through an object by a scintillator screen or charge couple device (CCD) [Bee06]. The basic idea of NRad is illustrated in Fig 2.4. The radiography detector records a shadow image or projection of the object on the detector plane. This information contains the internal details of the object under the investigation, in the form of different intensities of radiation reaching the detector [Rou03].

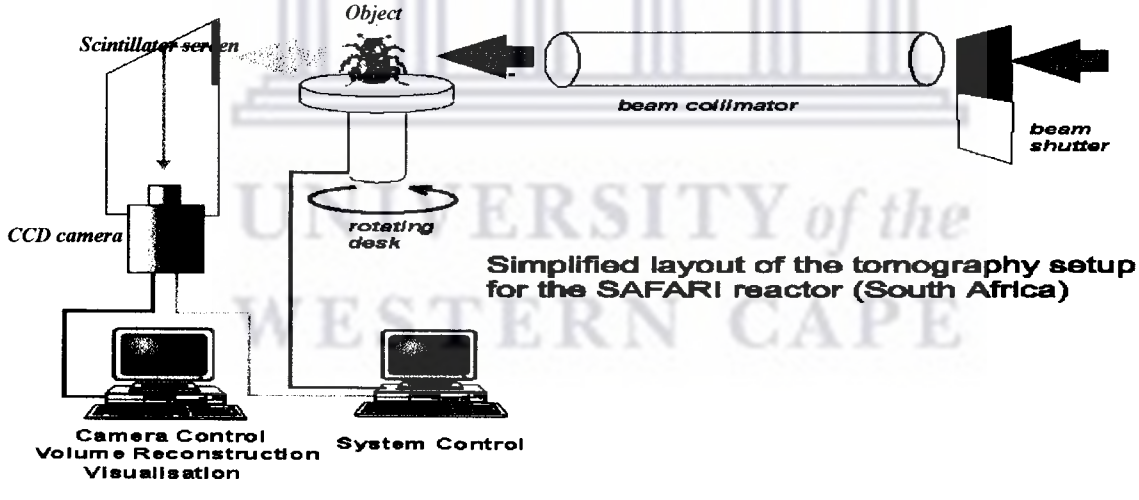

Fig 2.4. *Simplified layout of neutron tomography/ radiography (NRad) at NECSA [Rou03].*

Different radiation intensities that result are due to the attenuation[7] of radiation by the object and this depends on the type of radiation, material thickness, material density and material cross-section of the radiation used. The image or radiograph contains the information of the structure and composition of the object. In the case of thermal neutron radiography, the attenuation of the

[7]The amount of radiation absorbed and scattered by the material.

neutron beam is due to the scattering or absorption of neutrons with the nuclei of the atoms in the object material [Rou03]. NRad is created on an object or material that is subjected to the neutron beam.

2.5.3 Time-of-flight (TOF) technique

This technique is based on the simultaneous measurement of the velocity and energy of the detected particle. In the case of neutron detection, the neutron velocity is derived from the time to traverse a flight path of length l $(v = l/t)$ between [Cie82, Tes95] the point of origin of the neutron source (target) and the neutron detector. Obviously the time of origin of the neutron can only be known in a pulsed system, as would be the case for the PI^3 system [Fra06].

CHAPTER 3

Research Design and Methology

In Chapter 2, section 2.1, the literature review discussed the various neutron production techniques that differ in their characteristics in terms of their advantages and disadvantages.

In this study the Plasma Immersion Ion Implantation (PI^3) technique is used to produce neutrons. In this chapter the various components of the PI^3 processes and experimental setup of neutron detection are discussed.

3.1 The Plasma Immersion Ion implantation (PI^3) facility at NECSA

The Necsa plasma laboratory was used in this study. The PI^3 facility has been used for a number of industrial applications as mentioned in section (2.2.5), but in this study the facility was used for the surface modification of the target in order to generate neutrons from the D-D fusion reaction. The available equipment of the facility is schematically shown in Fig 3.1.

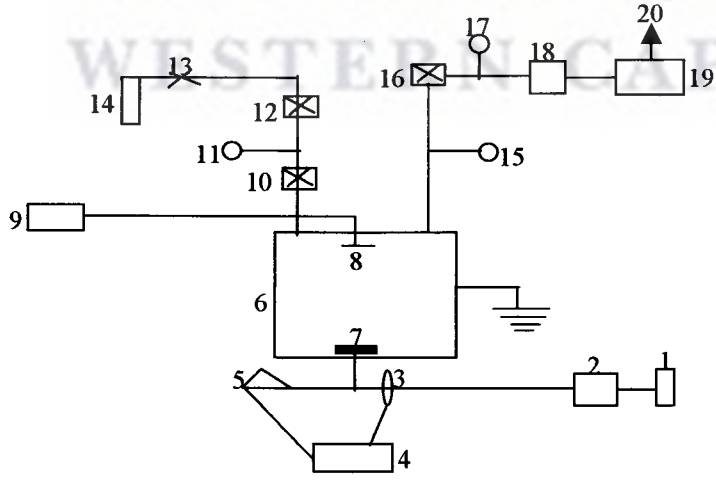

Fig 3.1. *Schematic representation of the PI^3 technique at NECSA: 1. Pulser generator. 2. High voltage pulse compressor. 3. Current probe (Rogowski coil). 4. Oscilloscope. 5. High voltage probe. 6. Plasma/ vacuum chamber. 7. Cathode and target stage. 8. Radio Frequency (RF) antenna. 9. RF power (adapted induction furnace). 10. Needle valve. 11. Pressure meter (gas flow into needle valve) 12. Piezoelectric gas leak valve. 13. Gas pressure regulator. 14. Gas bottle (deuterium/ tritium). 15. Pressure meters. 16. Buffer valve. 17. Pressure meter (vacuum pump). 18. Turbo molecular + rotary vane vacuum pump. 19. Fume cupboard. 20. outside (atmosphere).*

3.1.1 Physical layout

In Fig 3.1 above and 3.2 below; the plasma chamber which opens from the bottom in order to place the target on the cathode (shown in Fig 3.3) is illustrated. The digitizing 400 MHz oscilloscope shown in Fig 3.1 and Fig 3.7 is used to display the shapes of the voltage and current pulse signals registered by a high voltage probe and Rogowski coil respectively [Hon05].

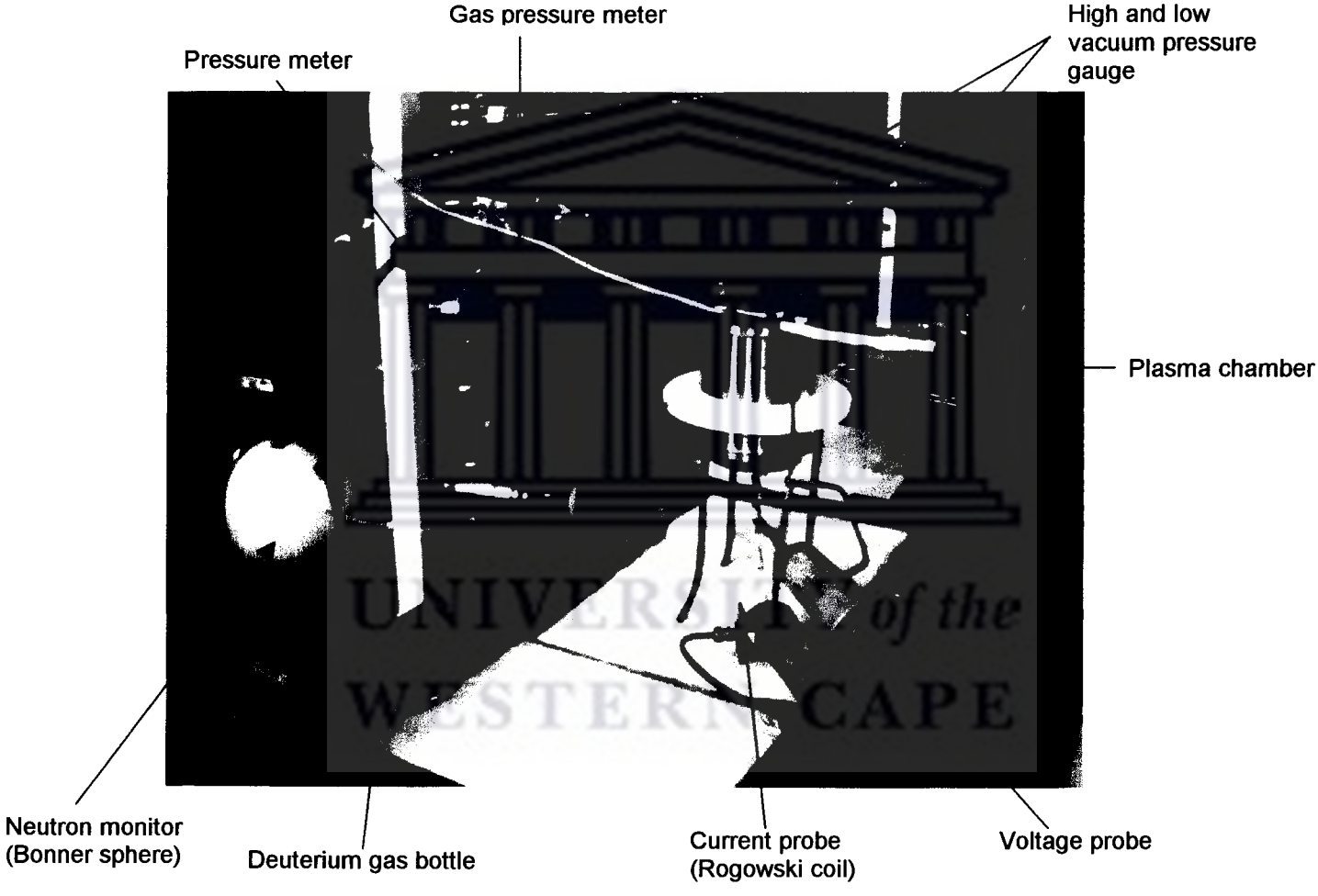

Fig 3.2. *Photograph of plasma chamber, voltage probe, current probe, deuterium gas bottle, neutron monitor and pressure gauges.*

- **Plasma/ Vacuum chamber**

The plasma experiments require a chamber to support the confined plasma source [Sach02]. In this study the bulk plasma experiment is conducted in a small cylindrical stainless steel chamber (see Fig 3.2) with a radius of 5.3 cm and a height of 12.5 cm. The system chamber is placed vertically as shown in Fig 3.3 so that the target can be placed on the target stage below the insulator cap. The insulator cap is used to prevent arcing at the edges of the terminal. It is also used for supporting the target and to prevent it from being dislodged from the stage during the experiment. The deuterium gas inlet and outlet are also shown in Fig 3.3. Plastic bolts were used to fasten the insulated cathode plate to the chamber.

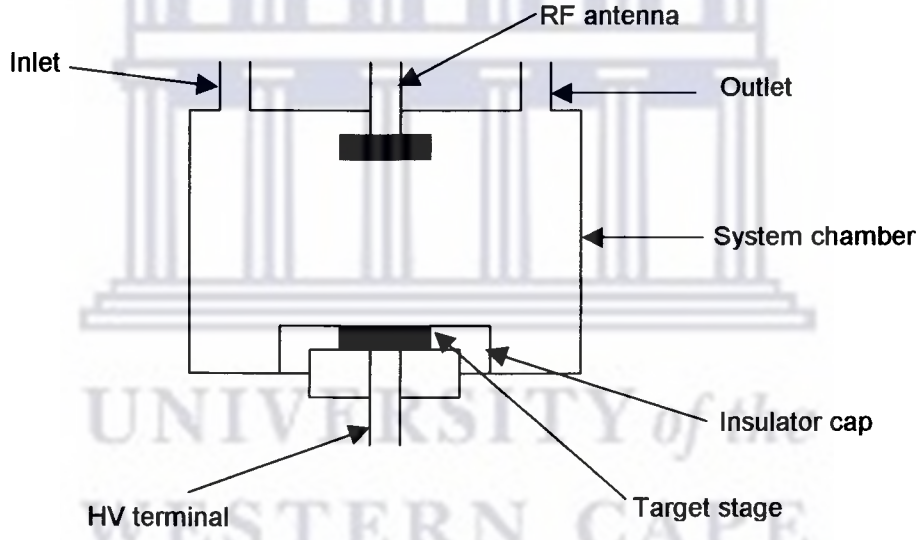

Fig 3.3. *Schematic representation of the plasma chamber.*

- **Needle valves**

Most of the needle valves consist of a movable piston with an optically flat sapphire, which forms a variable seal completely free from friction, seizing and shear [Tec96]. They are used for controlled admittance of fine gas flows. Movement of the position of the needle or the sapphire piston performs the fine adjustment of the gas. In this study, the movement of the needle is

controlled through a threaded shaft or a threaded shaft-and-lever mechanism. The needle valve of a model 28335 B1 Leybold-Heraeus was used in this study and is shown in Fig 3.4.

Fig 3.4. *Photograph of needle valve.*

The valve consists of different settings that depend on how much the shaft has been moved/rotated. The conductivity of a needle valve depends on the viscosity of the gas to be admitted into a vacuum chamber.

- **Vacuum pumps**

When selecting the most appropriate vacuum system for a neutron generator the following important factors should be taken into consideration:

i. The value of the ultimate pressure to be attained because the aim of all vacuum systems for a neutron generator is for the deuteron ions to reach the target without collision. This is maintained by working at low pressure, as is required by the PI^3 processes.
ii. Gas intake (due to leakage, the ion source, etc) to be accounted during the run of the experiment.
iii. Economic consideration such as the greatest possible simplicity in handling the pumps and the entire vacuum system (start, stop) [Tec96].

The facility consisted of the combination of a turbo molecular + rotary vane (model: TSH 172) and rotary vane (model: DUO 008 B) pumps in order to obtain the ultimate pressure below 10^{-4} Pa that is necessary for ensuring a pure gas environment. The photos of these pumps are shown in Fig 3.5.

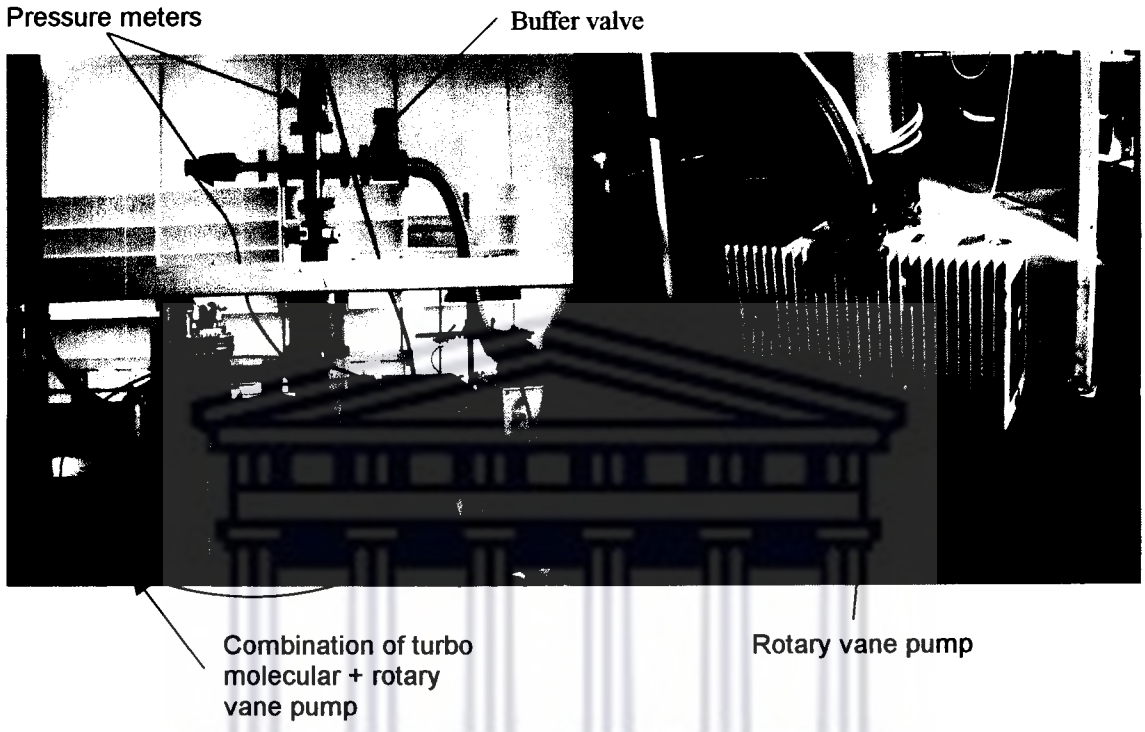

Fig 3.5. *The photos of the turbo molecular + rotary vane pump and rotary vane pump.*

The working principles of these pumps, as well as the most important details of the operation of vacuum systems containing the above combination of pumps is not to be discussed in this thesis.

- **Gas bottle**

As seen in Fig 3.2 the system used a small cylindrical gas bottle. In this study, the deuterium gas is contained in the gas bottle that is compressed to a very high pressure of 3500 kPa. The deuterium gas is used for the purpose of deuterating the target so that the new material can be formed (e.g. YD_x where Y is the target material, D is the deuterium and the YD_x a new material).

- **Pressure meters**

In order to monitor the vacuum status or gas pressure in the system there are pressure meters at different locations as seen in items 11, 15 and 17 in Fig 3.1. Gas pressure, after the gas has passed the piezoelectric gas leak valve, but before it is introduced into the plasma chamber was measured by the blue box (model: TFG 031) item (c) in Fig 3.6. The vacuum status inside the plasma chamber was measured by the cold cathode gauge (model: FKG 010) item (a) in Fig 3.6. The buffer (model: S20488), shown in Fig 3.5 (item 18 in Fig 3.1) is used to slow down the gas flowing from the plasma chamber to the pumping system. In between the buffer and the vacuum pump, the red box (model: CM 031) item b in Fig 3.6 was used to measure the gas pressure to the vacuum pump. The values of the pressure were taken from the pressure meter value displays shown in Fig 3.6.

Fig 3.6. *Photo of the different pressure meters value display. (a) Pressure inside the chamber display. (b) Pressure of molecular + rotary vane vacuum pump display. (c) Pressure of the gas before entering the chamber display.*

In summary, a differential pumping system shown in Fig 3.7 below was used to allow the continuous flow of gas in a system.

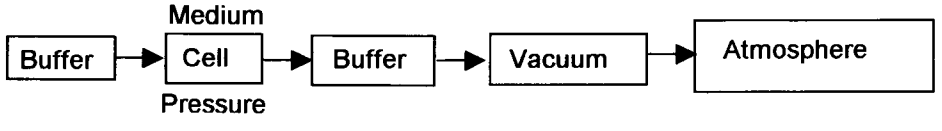

Fig 3.7. *Illustration of the differential pumping system.*

- **Radio frequency (R.F) power**

There are several plasma sources commonly used in PI^3 systems. Each has its own advantages and drawbacks. For instance, an electron cyclotron resonance (ECR) source can deliver a high plasma density but is relatively expensive [Chu97]. Therefore, a more economical capacitively coupled rf system was chosen for our facility. In our facility, an rf power source (model: VDGPT19) is used to generate the plasma. The rf plasma source is mounted onto the central part of the top of the plasma chamber and the rf power is fed through the rf antenna as it is shown in Fig 3.1 in item 8. The rf system of our facility is shown in Fig 3.8 below:

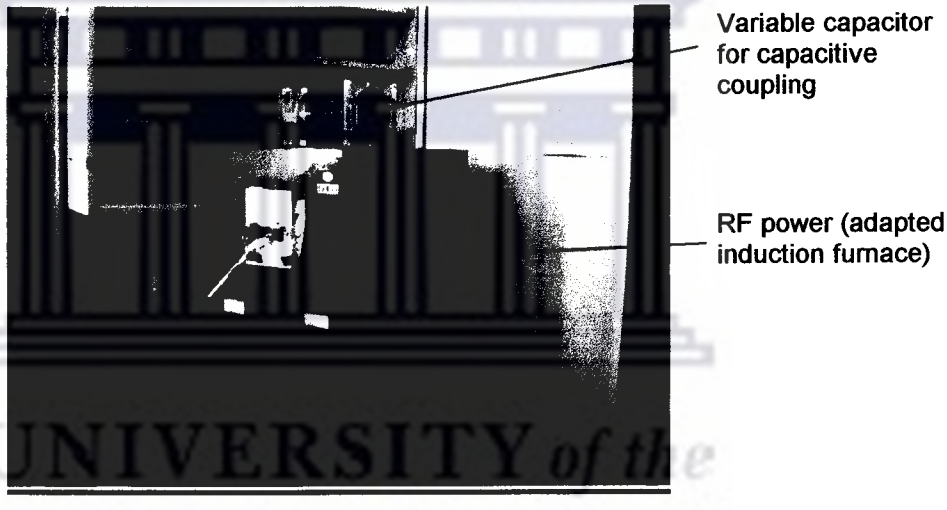

Fig 3.8. *Photograph of radio frequency (rf) power.*

The inductively coupled rf plasma source [Chu97] was used in this study because of the following advantages:

i. Relatively pure plasma due to electrodeless discharge;
ii. Reasonably high plasma density;
iii. Minimal contamination;
iv. Small substrate damage;
v. Higher atomic ion ratio and multiply charged ion content (higher plasma chemical activity);
vi. Suitable for active gases.

• High voltage pulse power supply

Ion implantation is usually performed at a high implantation voltage, low implantation temperature, and low working gas pressure [Chu97] as was mentioned in section 2.2. There are two primary methods to generate high voltage pulses. The first means is to employ an on-off switch in conjunction with a pulse-forming network (PFN) to generate the pulses [Xiu99]. The system used to perform this purpose in our facility is shown in Fig 3.9 which are; items labelled 1 and 2 when referring to Fig 3.1.

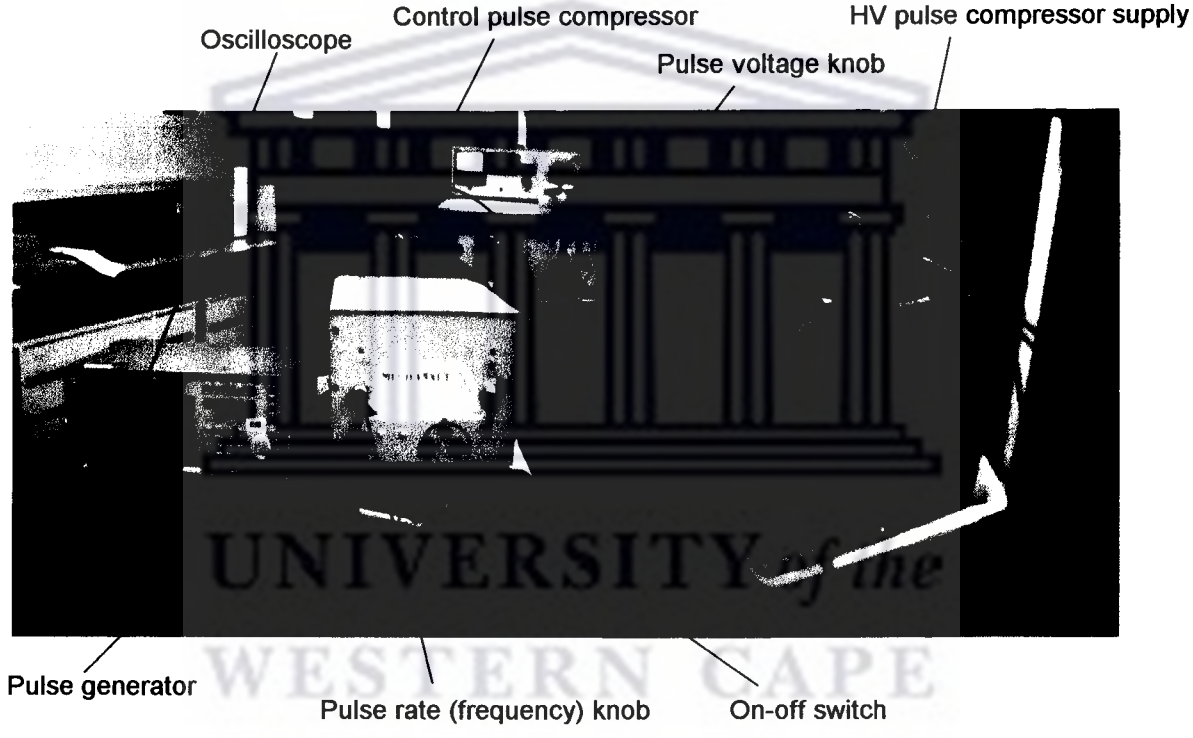

Fig 3.9. *Photograph of the components of high voltage pulse power supply.*

The resonant pulse power supply of our facility delivers a high voltage pulse with fast rise time (<1μs), sustaining the high voltage (HV) for several μs (~ 40μs) at high repetition rate up to 300 Hz and delivers up to 2 joules of energy.

- **Neutron monitor**

In order to verify that the fusion reaction occurred, nuclear radiation should be present; i.e. 50% of fusion decays to $^3He + n$, 50% to $T + p$ and 0.00001% to $^4He + \gamma$ [Fra06]. In this study, the neutron monitor (model: 12 – 4 count rate-meter) shown in Fig 3.2 was used to verify whether the fusion reaction has occurred or not. The response from the neutron monitor is discussed in Chapter 4 section 4.1.1.

3.1.2 Sample design/ Target design

Different substrates/ targets materials such as copper, titanium and nickel can be used. However, in this study only a titanium target was considered. Some other target configuration such as wire, mesh or rod may be used, but it is very important to note that the target must satisfy the characteristics discussed in section 3.2. The results and discussion of the implantation of deuterium ions into a titanium target are presented in section (4.1.4).

3.2 Sample/target characteristics

Generally, in all Plasma Immersion Ion Implantation the material used as a substrate/target must satisfy the following characteristics:

- The target can be of any configuration such as a thin disc, a rod, mesh or a wire;
- It must be a material that is good at keeping the deuterium atoms for a long period of time (e.g. it should not disorb it);
- It must be a conductor; and
- Be capable of withstand high voltage (HV) power deposition.

3.2.1 Common ground of Plasma Immersion Ion Implantation techniques

As discussed in section 2.2, in all Plasma Immersion Ion Implantation the surface of a substrate is immersed in a plasma environment and a relatively high substrate bias-voltage is applied. In this study, the substrate bias was pulsed [And02]:

- To limit the sheath size when operating at high voltage (>10 kV) and low pressure plasmas;
- To allow the near-substrate region to be refilled with ions during the bias-off time; and
- To have an additional degree of freedom such as pulse length and duty cycle for the design of treatment processes.

3.3 Experimental setup for neutron detection

The experimental setup for the neutron detection in this study consisted of the following:

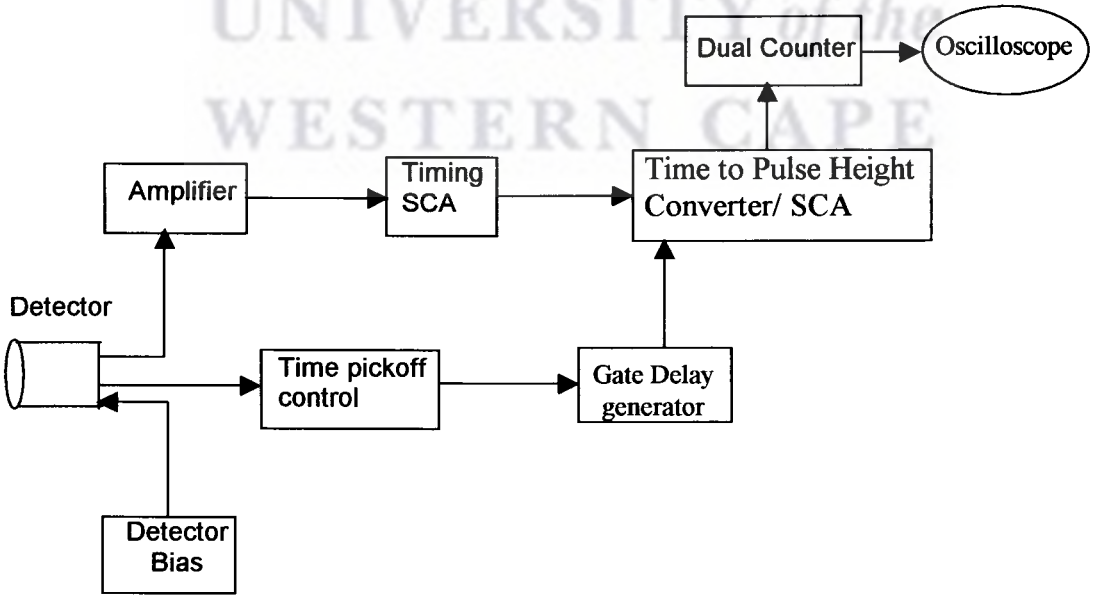

Fig 3.10. *Schematic diagram illustrating the electronics used for neutron detection for this experiment.*

a NE213 liquid scintillator detector, a detector HV bias (model 3002), an amplifier (model: 572 Ortec), a timing SCA (model: 520A Ortec), a time pickoff control (model: 403A Ortec), a gate and delay generator (model: 416 Ortec), a time to pulse height converter/ SCA (model: 467 Ortec), a dual counter timer (model 2071A) and a Tektronix 2465 300MHz oscilloscope. The system electronics for the experimental setup is illustrated in Fig 3.10.

- **Detector**

The detector used in this study was NE213 liquid scintillator detector which is an organic scintillator. In this type of detector, the energy of the incoming radiation passes through an organic solvent and is absorbed (the organic solvent consists of a small amount of scintillation material added to it), by exciting the electron in the scintillating material into one of a number of excited states. During this time, the emission of light results [Kno00]. The detector was connected to a photomultiplier tube (PMT) and preamplifier as illustrated in Fig 3.11 below. In this study, only one detector was used which was placed next to the plasma chamber. The number of counts at different target bias voltages is presented in Chapter 4, section 4.1.

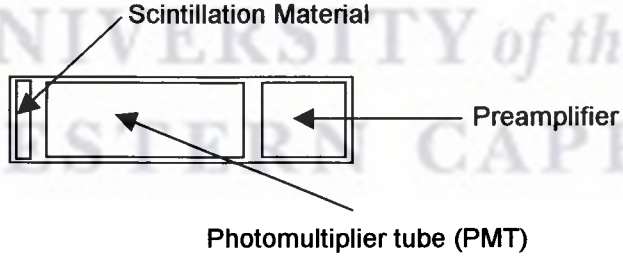

Fig 3.11. *Schematic presentation of the connection of the NE213 liquid scintillator detector to the photomultiplier tube (PMT) and preamplifier.*

3.3.1 Background measurements

The detector background arises from primary cosmic radiation, which can be either of galactic or solar origin, or natural radioactive decays e.g. ^{40}K, Th and U. Cosmic radiation is made up of charged particles and heavy ions with

extremely high kinetic energies. When such particles interact with the atmosphere (as shown in Fig 3.12), a large number of secondary particles are produced. This includes the production of pi and mu mesons, electrons, protons, neutrons and electromagnetic photons with energy ranges up to hundreds of MeV [Kno79].

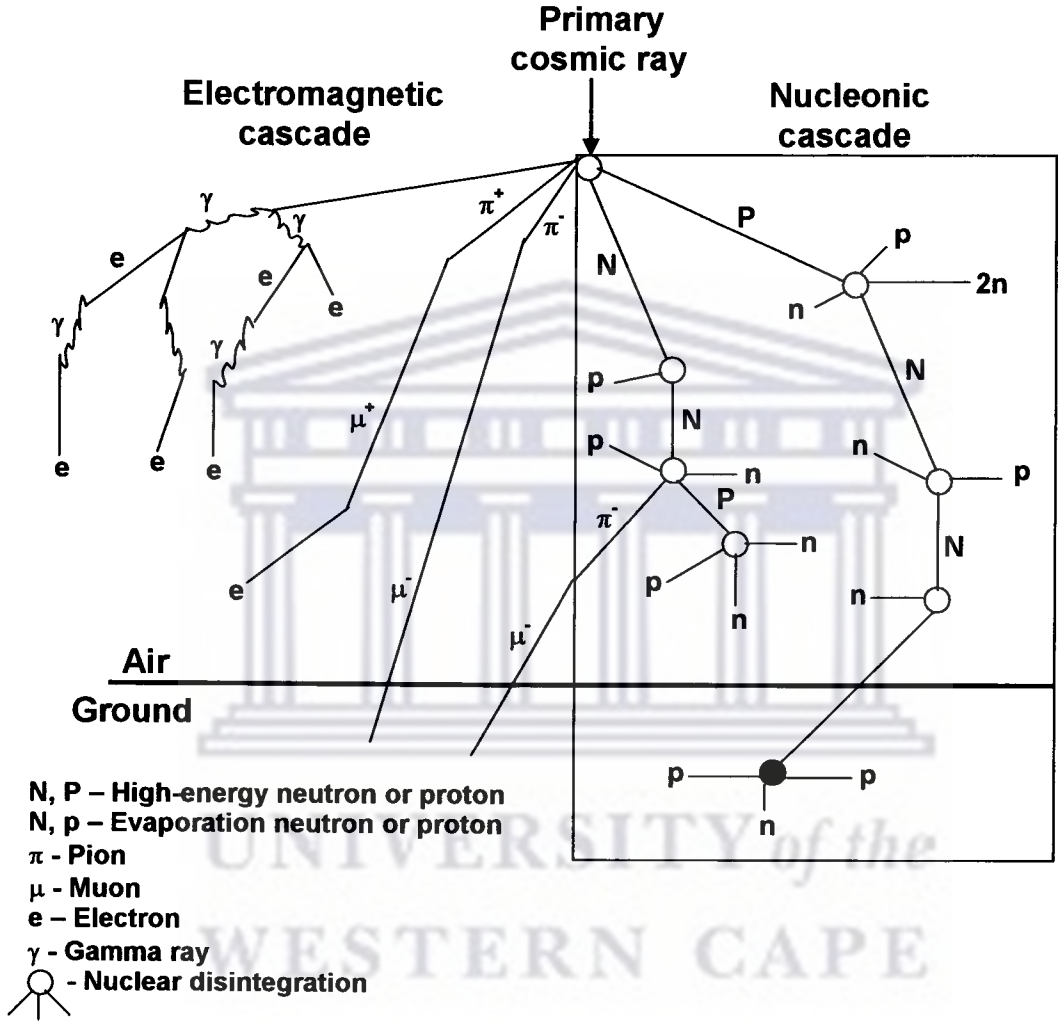

Fig 3.12. *Schematic presentation of the propagation of secondary cascade through the atmosphere [Dar01].*

The radiation discussed above, reaches the earth's surface and creates the background pulses in the detector.

In this study, the background radiation was traced by counting the number of counts for 1000 s when the system was switched off. From the average value of the background counts, the total number of counts was found (see equation

4.3). The results and the importance of background measurements are presented and discussed in section 4.1.2

3.4 Data collection processes

Data was collected every time before the experimental parameters were changed. The procedure used was to look at the different readings such as target maximum bias voltage, substrate current and number of counts on the dual counter. These readings were written down immediately before the pulse voltage was changed. The tables for different relationship of parameters during neutron detection experiments are presented in Chapter 4 section (4.1) as the results of this study.

3.5 Limitations and gaps in the data

In this thesis, our aim is to present the exact data. The data presented on the results in section 4.1 has the following limitations:

- Limited range of pressure (4 to 5 Pa).
- The radio frequency voltage below 50 and pulse frequency below 250 Hz since above these values, it was impossible to read the maximum pulse voltage in our system due to plasma instabilities and arcing.
- Peak pulsed voltage limited to less than 25 kV due to limited ability of the present power supply.

CHAPTER 4

Results: Presentation and Discussion

In this chapter, the most important aspects of the results such as description of main results, discussion of main trends and the summary of the main results are presented.

4.1 Description of main results

In this section the results of the neutron monitor, background measurement, predicted and calculated number of neutrons produced and the implantation of deuterium ions into titanium target results are presented.

4.1.1 Results of neutron monitor (Bonner sphere)

The neutron monitor (see Fig 3.2) was found to be sensitive to any type of signal that arose during the experiment. Our aim was to detect the neutrons and not other signals due to spurious electronic signals. This forced us to use the NE213 liquid scintillator detector in order to detect the radiation coming from neutrons and gamma's that were produced at certain pulse voltages. The proportional counters discussed in section 2.4.2 were not used because they are sensitive to electromagnetic pulses from the pulsed HV system and could not be easily discriminated against. However, in an NE213 detector such signals were distinguished by the electronics of the detection setup used. The number of counts registed by the NE213 detector at each target bias voltage at different frequency are presented and discussed in the following sections.

4.1.2 Background measurements results

Background data presented here was collected when no radio frequency (RF) or high voltage (HV) was present.

Background measurements for 1000 seconds

Trial No.	No of counts (N)	Experimental mean $\langle X_e \rangle$	Distribution function $F(X)$
1	1 ± 1	4.5 ± 0.6	
2	3 ± 1.7	4.5 ± 0.6	F(1) = 0.1
3	2 ± 1.4	4.5 ± 0.6	
4	2 ± 1.4	4.5 ± 0.6	F(2) = 0.2
5	8 ± 2.8	4.5 ± 0.6	
6	4 ± 2	4.5 ± 0.6	F(3) = 0.1
7	7 ± 2.65	4.5 ± 0.6	
8	8 ± 2.8	4.5 ± 0.6	F(4) = 0.2
9	4 ± 2	4.5 ± 0.6	
10	6 ± 2.5	4.5 ± 0.6	F(6) = 0.1
			F(7) = 0.1
			F(8) = 0.2
			Normalized = 1

Table 4.1: *Background measurement results for 1000 seconds.*

The associated uncertainties of the background measurements (N) as shown in Table 4.1 were found by using the usual experimental standard deviation equation [Kno00]:

$$\sigma_{\exp} = \sqrt{N} \qquad \ldots. (4.1)$$

The uncertainty shown in column of $\langle X_e \rangle$ in Table 4.1 is calculated by using the following equation [Lin07]:

$$unc = \langle X_e \rangle \left[\frac{\sqrt{N_T}}{N_T} \right] \qquad \ldots (4.2)$$

Where *unc* is the uncertainty, $\langle X_e \rangle$ is the experimental mean and N_T is the total number of counts.

In order to know the total number of counts, the background radiation must be determined first so that the total number of counts can be determined by the following equation:

$$NC_{total} = NC_{\exp} - NC_{Background} \quad \ldots (4.3)$$

where $NC_{\exp}$ is the experimental number of counts and $NC_{Background}$ is the background radiation. The parameters $\langle X_e \rangle$ and $F(X)$ shown in Table 4.1 are often used in data description, and they are defined in Appendix D. The distribution function chart for the data given in Table 4.1 is illustrated in Fig 4.1.

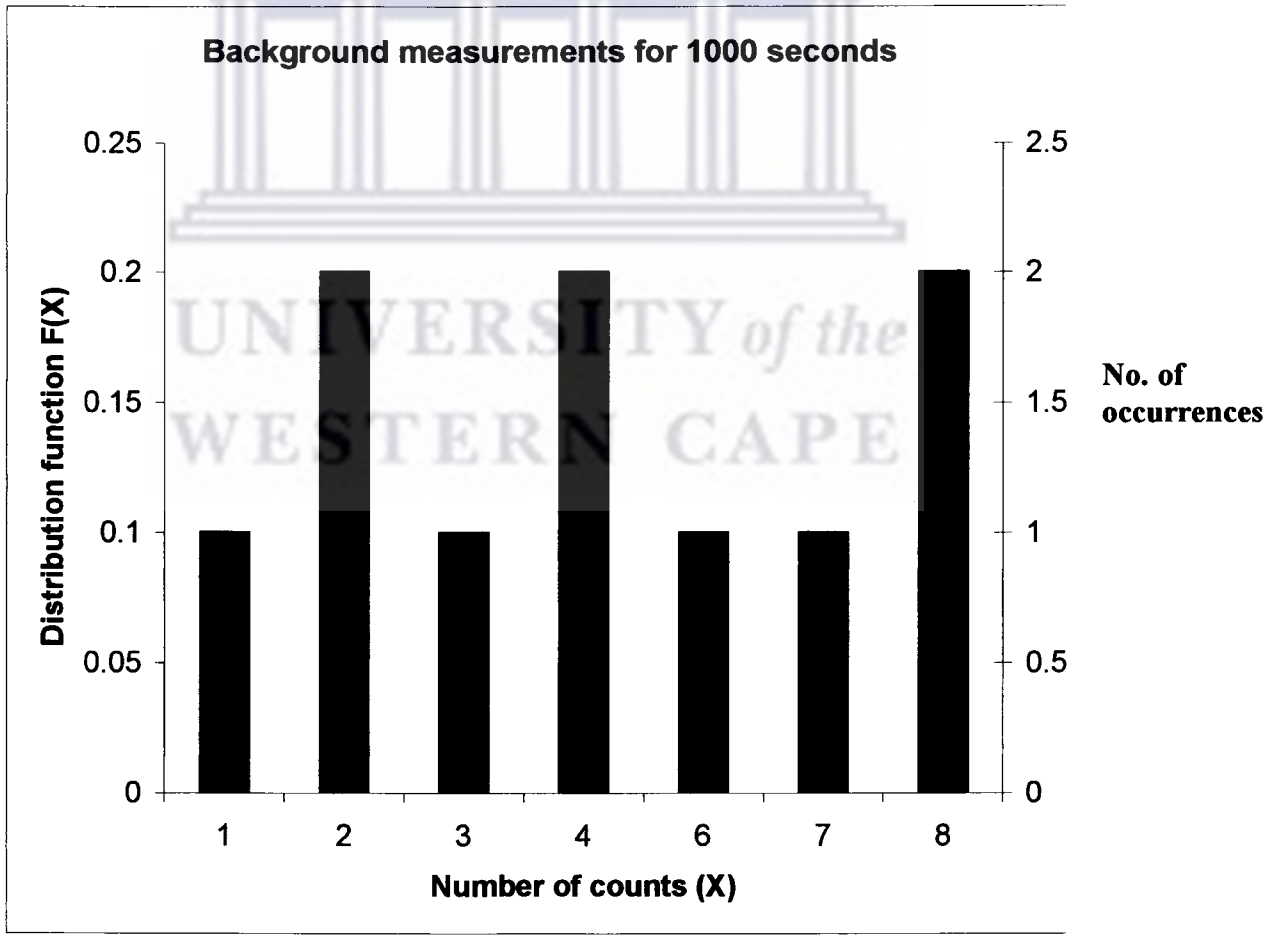

Fig 4.1: *Distribution function for data given in Table 4.1.*

The relative shape of the distribution function chart shown in Fig 4.1 indicates qualitatively the amount of internal fluctuation in the data given in Table 4.1.

4.1.3 Predicted and calculated number of neutrons produced

In this study, one NE213 detector of radius, r_d = 3.65 cm, was used to detect the radiation produced such as neutrons and photons. The NE213 detector was placed at a certain distance, d_d = 5.3 cm from the plasma chamber of radius, r_c = 5.3 cm, as is shown in Fig 4.2.

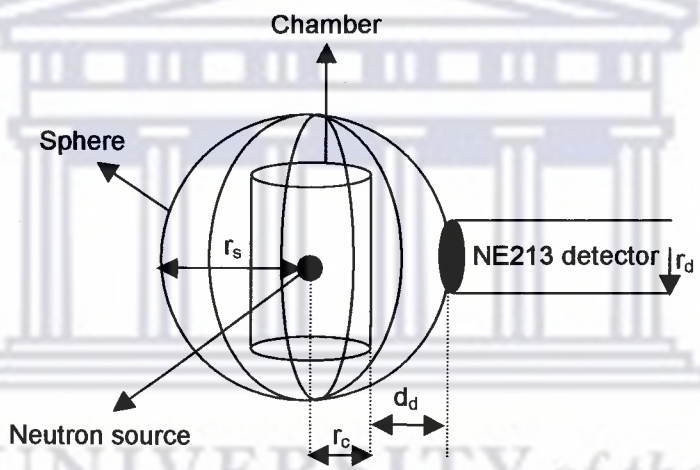

Fig 4.2: *A diagram showing the distance between the radiation source and detector.*

In order to predict the number of radiation particles produced at a specific target maximum bias voltage, a spherical model with radius r_s was assumed (see Fig 4.2). This assumption was made so that the ratio β of the surface area of a sphere $\left(4\pi r_s^2\right)$ to the area of a detector surface $\left(circle = \pi r_d^2\right)$ could be derived from basic principles that is;

$$\beta = 4\left[\frac{(r_c + d_d)}{r_d}\right]^2 = 4\left(\frac{r_s}{r_d}\right)^2 = 23.3 \qquad \ldots (4.4)$$

The value of β above is important because it is used in predicting the number of radiation particles produced (N_p) which is given by [Fra06]:

$$N_p = 4(NC_{total})\left[\frac{(r_c + r_d)}{r_d}\right]^2 = 4(NC_{total})\left(\frac{r_s}{r_d}\right)^2 = \beta(NC_{total}) = 23.3(NC_{total}) \quad \ldots (4.5)$$

where NC_{total} is the total number of counts after background subtraction (see equation 4.3). The term β is involved in equation 4.5 because in the PI[3] processes, the radiation particles such as neutrons and photons are produced isotropically that is; they are produced in all directions (e.g. no preferred angle).

Apart from N_p, the calculated total number of fusion reactions that occurred (NF_{ct}) can also be determined by using the following equation [Fra06]:

$$NF_{ct} = \Delta N.f.t_m \quad \ldots (4.6)$$

where f is the frequency of the HV power supply, t_m is the measurement time, which is 1000s in this study, and ΔN is the number of fusion reactions during each pulse given by Uhm and Lee [Uhm91] as:

$$\Delta N = 2\left[\frac{\sqrt{E}n_0\sigma(E)I_{ion}\Delta r\tau}{45e}\right] \quad \ldots (4.6.a)$$

where n_0 is the density of deuterium atoms in the titanium target, which in this study was assumed to be $(n_0 = 1\times10^{18}\,atoms/cm^3)$. The term I_{ion} is the average ion current per pulse; τ is pulse length using an average $10\mu s$ in our results and the ion kinetic energy E at the target surface is in keV units. The term (Δr) is the penetration depth of the deuterium ions into the titanium target, which was determined using the SRIM program [Bie03, Zie77]. The

term $\sigma(E)$ in equation (4.6.a) is the cross section of the nuclear fusion in cm^2, which is given by Huba [Hub02] as:

$$\sigma(E) = \frac{\left[(A_4 - A_3 E)^2 + 1\right]^{-1} A_2}{E\left[Exp\left(A_1 E^{1/2}\right) - 1\right]} \quad \ldots (4.6.b)$$

where the coefficients $A_1 = 47.88$, $A_2 = 482$, $A_3 = 3.08 \times 10^{-4}$ and $A_4 = 1.177$ for the D-D reaction. The results for the relationship of the above-mentioned parameters are presented in tables 4.2 – 4.6 in section 4.1.4.

Furthermore, in this study, the calculated total number of fusion neutrons over a solid angle of 4π per 1000 s in the detector are presented as the optimistically predicted (P_o) which is given by [Fra06]:

$$P_0 = \frac{NF_{ct}}{\beta} \quad \ldots (4.7)$$

where (NF_{ct}) and β are described as in equation 4.6 and 4.4, respectively. It is emphasised that the n_0 value is taken/assumed as $n_0 = 1 \times 10^{18}\ atoms/cm^3$ for the P_0 results presented in Tables 4.7 – 4.11. The pessimistically predicted, P_p, results are also presented in Tables 4.7 – 4.11, but in this case the n_0 value was assumed to be $n_0 = 1 \times 10^{16}$. The assumed large values of n_0 will be discussed in detail in section 4.2. With this assumption one could easily recognize that the pessimistically predicted P_p results can be given by the following simple equation:

$$P_p = 10^{-2}\left(\frac{NF_{ct}}{\beta}\right) = 10^{-2} P_0 \quad \ldots (4.8)$$

whereby the factor 10^{-2} results from the ratio of the assumed density of P_p to that of P_0. The above simple equation simplifies the repetition of the

calculations because all the conditions for $E(kV)$, $\Delta r(cm)$, $\sigma(cm^2)$ and $I_{ion}(A)$ are the same, except the n_0 value that will only change the ΔN and NF_{ct} values by a factor of 10^{-2}. The results for the P_p and P_0 are presented in Tables 4.7 - 4.11.

4.1.4 Implantation of deuterium atoms into titanium target results

In this section, the results at different frequencies for the relationship of the parameters mentioned in the above section are presented in the following Tables. The associated uncertainties shown in the columns of $NC_{\exp}$ in Tables 4.2 – 4.6, were found by using equation 4.1 discussed earlier. The uncertainties shown in columns of NC_{total} in Tables 4.2 – 4.11, were found by using equation 4.2 whereby the following conditions were made, that is; $\langle X_e \rangle$ = NC_{total} and N_T = $NC_{\exp}$.

Trial #	$E(kV)$	$\Delta r(cm)$	$\sigma(cm^2)$	$I_{ion}(A)$	$NC_{\exp}$	N_p	NC_{total}	ΔN	NF_{ct}
1	10.63	1.18E-05	1.02E-29	0.04	3 ± 2	0	0 ± 0	4.44E-05	2.22E+00
2	12.19	1.34E-05	2.27E-29	0.06	5 ± 2	12	0.5 ± 0.2	1.75E-04	8.77E+00
3	14.38	1.52E-05	5.50E-29	0.06	5 ± 2	12	0.5 ± 0.2	5.48E-04	2.74E+01
4	16.25	1.73E-05	1.00E-28	0.13	18 ± 4	315	13.5 ± 3	2.48E-03	1.24E+02
5	18.13	1.90E-05	1.65E-28	0.14	20 ± 4	361	15.5 ± 3	5.24E-03	2.62E+02
6	20.94	2.15E-05	3.04E-28	0.20	23 ± 5	431	18.5 ± 4	1.69E-02	8.44E+02
7	22.50	2.29E-05	4.04E-28	0.23	24 ± 5	454	19.5 ± 4	2.78E-02	1.39E+03

Table 4.2: *Implantation of deuterium atoms into titanium target results. All measurements were recorded at frequency of 50 Hz, with an RF voltage of 40 V and a chamber pressure of 20 mbar.*

Trial #	$E(kV)$	$\Delta r(cm)$	$\sigma(cm^2)$	$I_{ion}(A)$	NC_{exp}	N_p	NC_{total}	ΔN	NF_{ct}
1	10.63	1.18E-05	1.02E-29	0.038	4 ± 2	0	0 ± 0	4.10E-05	2.05E+00
2	12.50	1.37E-05	2.62E-29	0.047	4 ± 2	0	0 ± 0	1.65E-04	8.24E+00
3	14.68	1.58E-05	6.10E-29	0.038	3 ± 1	0	0 ± 0	3.85E-04	1.92E+01
4	16.88	1.79E-05	1.20E-28	0.044	7 ± 2	58	2.5 ± 1	1.07E-03	5.34E+01
5	18.44	1.93E-05	1.78E-28	0.047	3 ± 1	0	0 ± 0	1.92E-03	9.61E+01
6	20.63	2.13E-05	2.86E-28	0.056	8 ± 3	81	3.5 ± 1	4.32E-03	2.16E+02

Table 4.3: *Implantation of deuterium atoms into titanium target results. All measurements were recorded at frequency of 50 Hz, with an RF voltage of 50 V and a chamber pressure of 18 mbar*

Trial #	$E(kV)$	$\Delta r(cm)$	$\sigma(cm^2)$	$I_{ion}(A)$	NC_{exp}	N_p	NC_{total}	ΔN	NF_{ct}
1	10.94	1.21E-05	1.02E-29	0.031	22 ± 4	408	17.5 ± 4	3.07E-05	7.68E+00
2	12.50	1.37E-05	3.42E-29	0.063	9 ± 3	105	4.5 ± 1	3.08E-04	7.69E+01
3	14.69	1.58E-05	9.14E-29	0.106	17 ± 4	291	12.5 ± 3	1.45E-03	3.63E+02
4	18.44	1.93E-05	1.41E-28	0.141	30 ± 5	594	25.5 ± 5	2.74E-03	6.84E+02
5	20.31	2.10E-05	2.05E-28	0.147	32 ± 5	641	27.5 ± 5	4.79E-03	1.20E+03
6	22.19	2.26E-05	2.68E-28	0.203	34 ± 6	687	29.5 ± 5	7.92E-03	1.98E+03

Table 4.4: *Implantation of deuterium atoms into titanium target results. All measurements were recorded at frequency of 100 Hz, with an RF voltage of 50 V and a chamber pressure of 18 mbar*

Trial #	$E(kV)$	$\Delta r(cm)$	$\sigma(cm^2)$	$I_{ion}(A)$	NC_{exp}	N_p	NC_{total}	ΔN	NF_{ct}
1	10.31	1.15E-05	8.48E-30	0.041	9 ± 3	105	4.5 ± 1	3.53E-05	3.53E+00
2	12.50	1.37E-05	2.62E-29	0.069	7 ± 2	58	2.5 ± 1	2.42E-04	2.42E+01
3	14.69	1.58E-05	6.12E-29	0.097	6 ± 2	35	1.5 ± 1	9.99E-04	9.99E+01
4	16.25	1.73E-05	1.00E-28	0.125	9 ± 3	105	4.5 ± 1	2.42E-03	2.42E+02
5	18.44	1.93E-05	1.78E-28	0.047	9 ± 3	105	4.5 ± 1	1.92E-03	1.92E+02
6	20.63	2.13E-05	2.86E-28	0.056	10 ± 3	128	5.5 ± 2	4.32E-03	4.32E+02
7	22.50	2.29E-05	4.04E-28	0.066	12 ± 3	175	7.5 ± 2	7.99E-03	7.99E+02
8	24.78	2.48E-05	5.80E-28	0.066	19 ± 4	338	14.5 ± 3	1.31E-02	1.31E+03

Table 4.5: *Implantation of deuterium atoms into titanium target results. All measurements were recorded at frequency of 200 Hz, with an RF voltage of 50 V and a chamber pressure of 18 mbar.*

Trial #	$E(kV)$	$\Delta r(cm)$	$\sigma(cm^2)$	$I_{ion}(A)$	NC_{exp}	N_p	NC_{total}	ΔN	NF_{ct}
1	10.63	1.18E-05	1.02E-29	0.028	9 ± 3	105	4.5 ± 1	3.07E-05	7.68E+00
2	13.13	1.43E-05	3.42E-29	0.063	10 ± 3	128	5.5 ± 2	3.08E-04	7.69E+01
3	15.94	1.70E-05	9.14E-29	0.084	12 ± 3	175	7.5 ± 2	1.45E-03	3.63E+02
4	17.50	1.84E-05	1.41E-28	0.091	11 ± 3	151	6.5 ± 2	2.74E-03	6.84E+02
5	19.06	1.99E-05	2.05E-28	0.097	12 ± 3	175	7.5 ± 2	4.79E-03	1.20E+03
6	20.31	2.10E-05	2.68E-28	0.113	10 ± 3	128	5.5 ± 2	7.92E-03	1.98E+03

Table 4.6: *Implantation of deuterium atoms into titanium target results. All measurements were recorded at frequency of 250 Hz, with an RF voltage of 50 V and a chamber pressure of 18 mbar.*

In the following tables the optimistic predicted P_0 and the pessimistic predicted P_p number of counts (as seen in the detector) relationship as in equation 4.6 are presented.

Trial #	$E(kV)$	P_0	P_p	NC_{total}
1	10.63	9.53E-02	9.53E-04	0.0 ± 0
2	12.19	3.76E-01	3.76E-03	0.5 ± 0.2
3	14.38	1.18E+00	1.18E-02	0.5 ± 0.2
4	16.25	5.32E+00	5.32E-02	13.5 ± 3
5	18.13	1.12E+01	1.12E-01	15.5 ± 3
6	20.94	3.62E+01	3.62E-01	18.5 ± 4
7	22.5	5.97E+01	5.97E-01	19.5 ± 4

Table 4.7: *Optimistic and pessimistic results of implantation of deuterium atoms into titanium target, all measurements at 50 Hz and RF voltage of 40 V at chamber pressure of 20 mbar.*

Trial #	$E(kV)$	P_0	P_p	NC_{total}
1	10.63	8.80E-02	8.80E-04	0 ± 0
2	12.50	3.54E-01	3.54E-03	0 ± 0
3	14.68	8.24E-01	8.24E-03	0 ± 0
4	16.88	2.29E+00	2.29E-02	2.5 ± 1
5	18.44	4.12E+00	4.12E-02	0 ± 0
6	20.63	9.27E+00	9.27E-02	3.5 ± 1

Table 4.8: *Optimistic and pessimistic results of implantation of deuterium atoms into titanium target, all measurements at 50 Hz and RF voltage of 50 V at chamber pressure of 18 mbar.*

Trial #	$E(kV)$	P_0	P_p	NC_{total}
1	10.94	3.30E-01	3.30E-03	17.5 ± 4
2	12.5	3.30E+00	3.30E-02	4.5 ± 1
3	14.69	1.56E+01	1.56E-01	12.5 ± 3
4	18.44	2.94E+01	2.94E-01	25.5 ± 5
5	20.31	5.15E+01	5.15E-01	27.5 ± 5
6	22.19	8.50E+01	8.50E-01	29.5 ± 5

Table 4.9: *Optimistic and pessimistic results of implantation of deuterium atoms into titanium target, all measurements at 100 Hz and RF voltage of 50 V at chamber pressure of 18 mbar.*

Trial #	$E(kV)$	P_0	P_p	NC_{total}
1	10.31	1.52E-0 1	1.52E-03	4.5 ± 1
2	12.50	1.04E+00	1.04E-02	2.5 ± 1
3	14.69	4.29E+00	4.29E-02	1.5 ± 1
4	16.25	1.04E+01	1.04E-01	4.5 ± 1
5	18.44	8.24E+00	8.24E-02	4.5 ± 1
6	20.63	1.85E+01	1.85E-01	5.5 ± 2
7	22.5	3.43E+01	3.43E-01	7.5 ± 2
8	24.78	5.62E+01	5.62E-01	14.5 ± 3

Table 4.10: *Optimistic and pessimistic results of implantation of deuterium atoms into titanium target, all measurements at 200 Hz and RF voltage of 50 V at chamber pressure of 18 mbar.*

Trial #	$E(kV)$	P_0	P_p	NC_{total}
1	10.63	3.30E-01	3.30E-03	4.5 ± 1
2	13.13	3.30E+00	3.30E-02	5.5 ± 2
3	15.94	1.56E+01	1.56E-01	7.5 ± 2
4	17.5	2.94E+01	2.94E-01	6.5 ± 2
5	19.06	5.15E+01	5.15E-01	7.5 ± 2
6	20.31	8.50E+01	8.50E-01	5.5 ± 2

Table 4.11: *Optimistic and pessimistic results of implantation of deuterium atoms into titanium target, all measurements at 250 Hz and RF voltage of 50 V at chamber pressure of 18 mbar.*

The graphs showing the relationship between NC_{total}, P_0 and P_p as a function of energy at different frequencies for the implantation of deuterium atoms into titanium target are presented in Fig 4.3 – 4.7. Note that when plotting the

predictions, events less than 1.0E-01 are plotted as 1.0E-01 since this is equivalent to zero counts monitored in the detector during a 1000 s counting time.

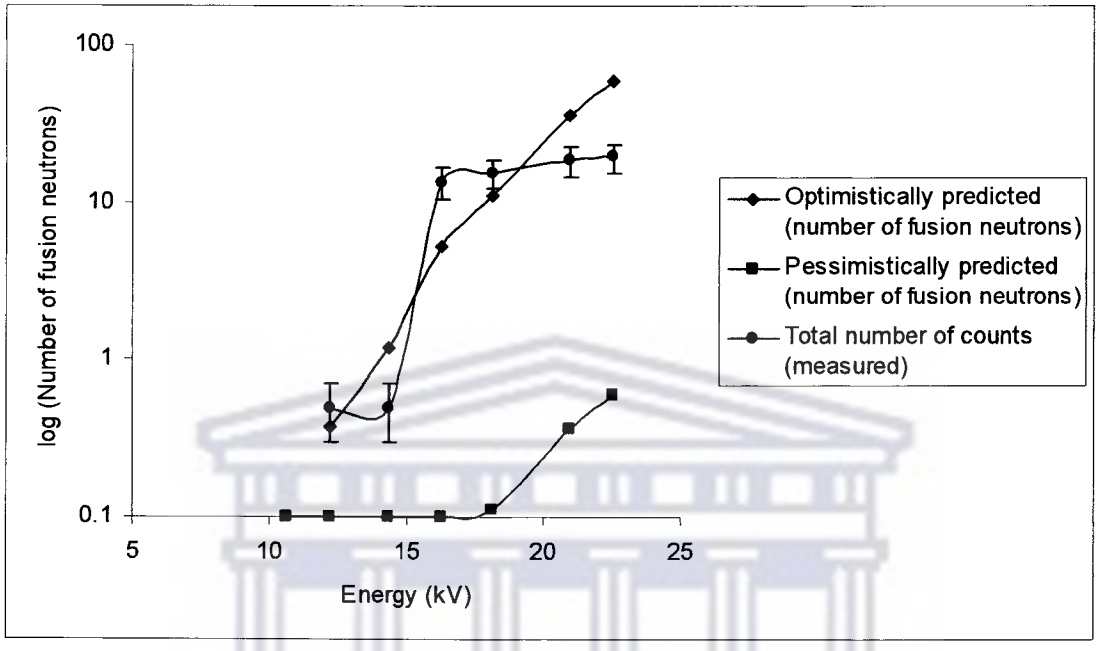

Fig 4.3: *Graph of number of fusion neutrons against energy for data in Table 4.7.*

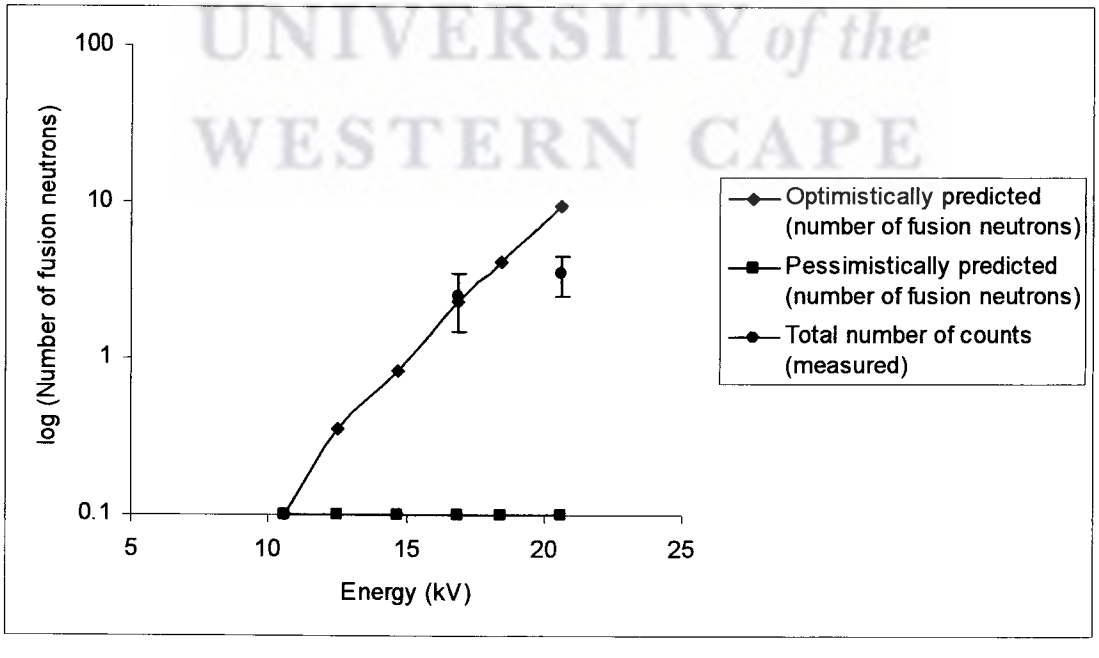

Fig 4.4: *Graph of number of fusion neutrons against energy for data in Table 4.8.*

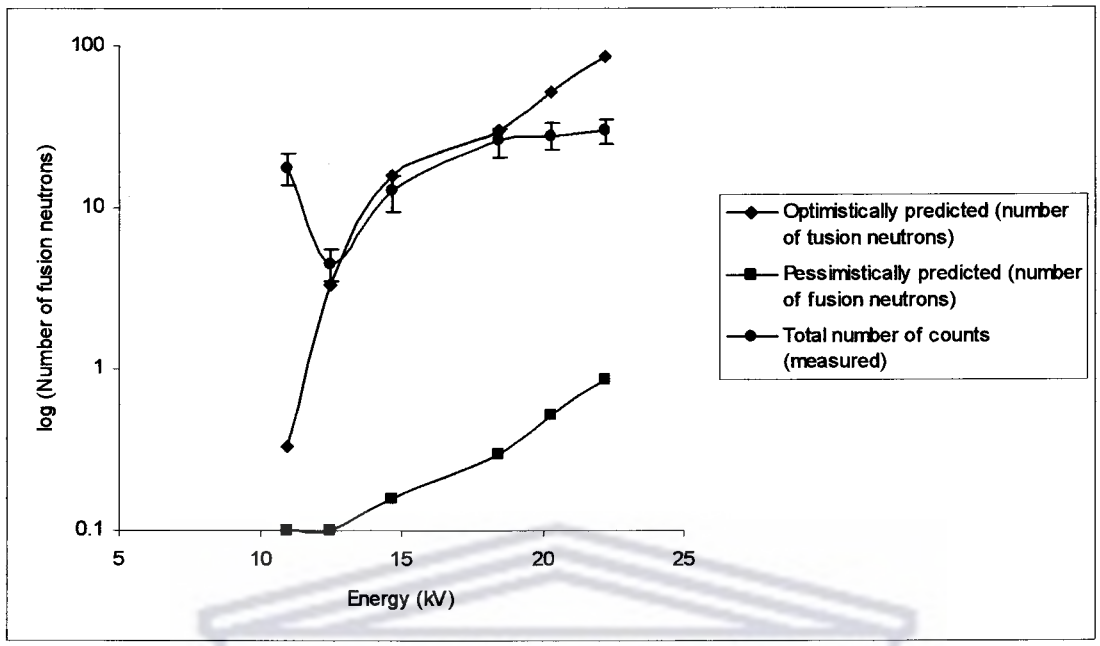

Fig 4.5: *Graph of number of fusion neutrons against energy for data in Table 4.9.*

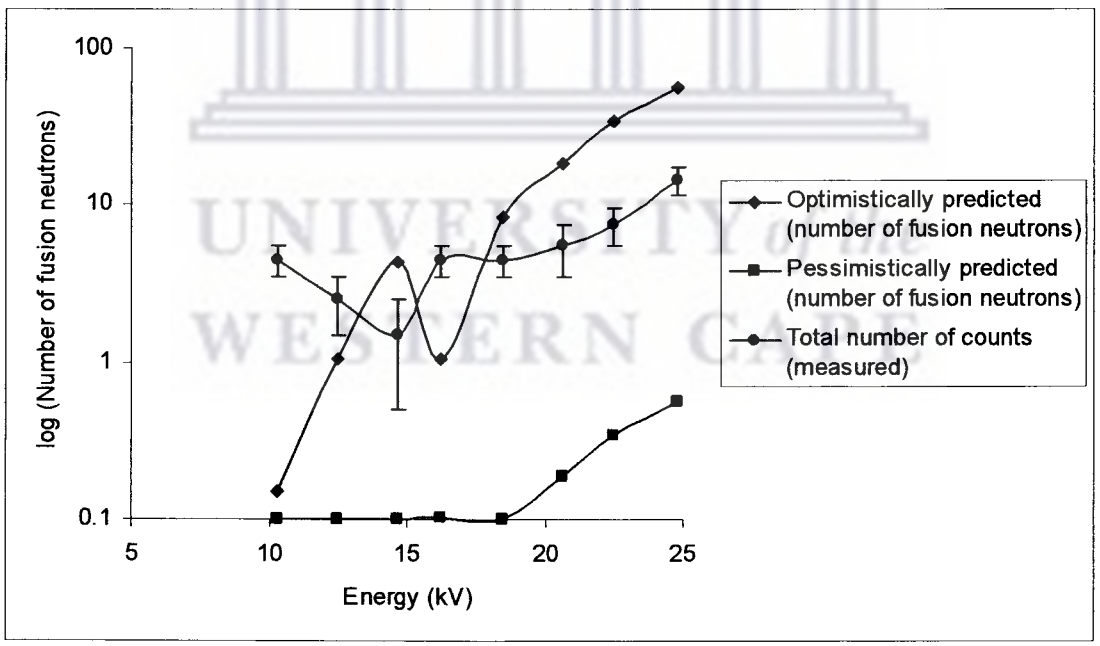

Fig 4.6: *Graph of number of fusion neutrons against energy for data in Table 4.10.*

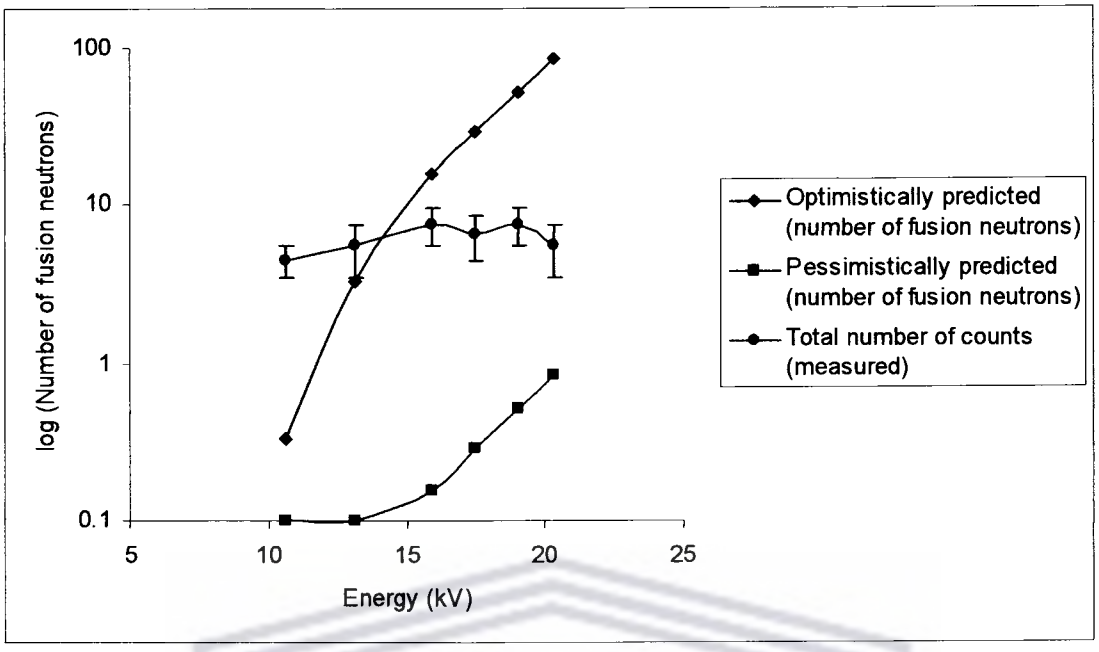

Fig 4.7: *Graph of number of fusion reaction occurred against energy for data in Table 4.11.*

4.2 Summary of the main results and discussion of main trends

In general, the results demonstrate that when the voltage is increased (in the pulse generator) the amplitudes of voltage and current pulses are also increased and the more the number of neutrons is observed. The results are optimistically and pessimistically predicted based on the following assumptions:

- The ion current (I_{ion}) was assumed to be constant, whereby the maximum value was used which was not necessarily the case at the time of peak voltage. As can be seen on the oscilloscope trace in Fig 4.8 that at maximum voltage pulse there is virtually no current.
- The voltage was not constant as it was considered in this study because there is a period of voltage increase during which current rapidly rose.

- It was assumed that voltage and current pulse trace was exactly the same for the measured time of 1000s.
- It was assumed that voltage and current are uniform for width of pulse τ (i.e. maybe use $\frac{1}{2}\tau$ or $\frac{1}{10}\tau$).

Fig 4.8: *Photograph of the oscilloscope showing the voltage peak (a) and current peak (b) on the y-axis against time on the x-axis.*

- Ion density of the deuterium atoms in the titanium target n_0 was not measured and it is complex to determine/ measure this value. It was assumed, based on nitrogen implantation research preformed with the same equipment. Unfortunately from nitrogen implantation research n_0 could be anywhere between 10^{14} – 10^{22} or even as low as 10^{9} based on depth profile analysis, but still an uncertainty of 1 – 2 orders of magnitude could result.
- Detection efficiency of the detector was not taken into consideration as only a correction for the solid angle was made.
- The penetration depth of deuterium ions into titanium target was calculated using the computer software SRIM. It could have been

measured using RBS or NRA (if time had been available for such measurements), and it was assumed to be uniform.

The results presented in this thesis, have the lack of neutron background measurement data with pulsed power supply and RF operating where the non-fusion gases such as argon or nitrogen gas could have been used so that the results could be compared to the fusion deuterium gas. Due to problems with the HV pulsed power supply only a few background measurements were performed using nitrogen gas, RF power on and pulsed HV at 15 kV, at 50 Hz and 100 Hz. The number of "neutron" counts measured in the neutron detector (NE213) was 7 and 8 respectively. In conclusion, the results for this project shows that the fusion reaction will only occur if the fusion gas such as deuterium is used, otherwise no fusion reaction will occur.

CHAPTER 5

Conclusions and Recommendations

In this chapter the conclusions based on the results of this study are made and future work on the study is also recommended.

5.1 Outlook

This study concludes that the PI^3 process is indeed a potential candidate for the production of neutrons. The neutron generator developed in this study is portable and reliable [Han91], that is; it is easily movable compared to the big accelerator such as Van de Graaff. The most important issue with regards to the system is its versatility [Chu97] in that it could also be used for other purposes such as applications mentioned in section 2.2.5. As far as this study is concerned the neutron source will be free from radiation hazards when the generator is switched off.

For the future work on the study the following are recommended:

- Employing a higher voltage power supply capable of delivering a higher voltage than the present one at an even higher frequency, in order to allow the fusion reaction to take place so that more neutrons can be generated.
- A popular approach such as using the Langmuir probes in order to asses/evaluate the ion density/plasma density in the processing chamber must be attempted [Chu97]. This may be better than assuming the plasma density as it was for this study.
- Improving the neutron detection probability in this technique, the neutron moderators such as polyethylene blocks with detectors placed inside them may surround the chamber for neutron detection rather than predicting the number of neutrons produced.

Appendix A

Plot of neutron production cross-section and the total yield of neutrons versus deuteron energy [Tec96].

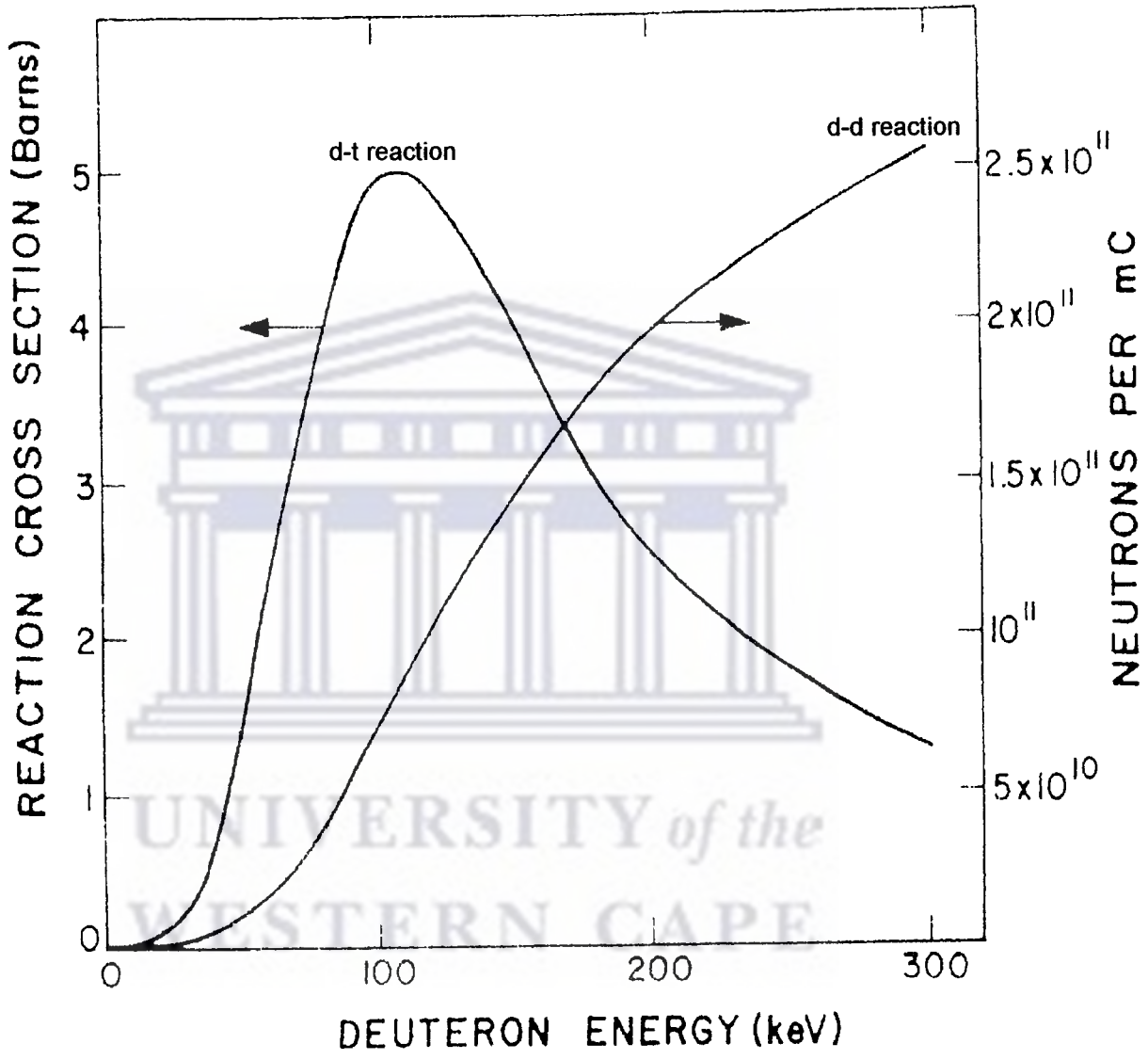

Appendix B

B-1

The data tables in B-1 and B-2 [Isb87] were found by using the "croscalc" program of which its input is as follows for D-T reaction and the input for D-D reaction is presented in B-2. After the input has been inserted the program runs and gives the values of Lab and centre of mass angle, Energy and cross-section.

Program input for D-T reaction

Mono-energetic neutron production
Label reaction by mass number of projectile and target
Projectile mass: 2
Target mass: 3
Neutron from the reaction $^{3}He(d,n)^{4}He$
Projectile energy or negative neutron energy at 0 deg (MeV): 0.02
Number of angles (negative if c.m.): 15
Angles, one by one. 1 –ve value for constant angle spacing: -10
Incident lab energy: 0.02 MeV

Data for D-T reaction

Laboratory System			Centre-of-mass System	
Angle (degrees)	Cross-section (mbarn)	Energy (MeV)	Angle (degrees)	Cross-section (mbarn)
Using 0.02 MeV in Legrendre Table				
0	4.699	14.36	0	4.6
10	4.698	14.356	10.11	4.6
20	4.693	14.342	20.21	4.6
30	4.686	14.391	30.31	4.6
40	4.676	14.289	40.39	4.6
50	4.663	14.251	50.47	4.6
60	4.649	14.208	60.53	4.6
70	4.634	14.16	70.58	4.6
80	4.617	14.109	80.6	4.6
90	4.600	14.056	90.61	4.6
100	4.583	14.004	100.6	4.6
110	4.566	13.954	110.58	4.6
120	4.551	13.906	120.53	4.6
130	4.537	13.864	130.47	4.6
140	4.525	13.827	140.39	4.6

B-2

Program input for D-T reaction

Mono-energetic neutron production
Label reaction by mass number of projectile and target
Projectile mass: 2
Target mass: 2
Neutron from the reaction $^{2}He(d,n)^{4}He$
Projectile energy or negative neutron energy at 0 deg (MeV): 0.02
Number of angles (negative if c.m.): 15
Angles, one by one. 1 –ve value for constant angle spacing: -10
Incident lab energy: 0.02 MeV

Data for D-D reaction

Laboratory System			Centre-of-mass System	
Angle (degrees)	cross-section (mbarn)	Energy (MeV)	Angle (degrees)	cross-section (mbarn)
		Using 0.02 MeV in Legrendre Table		
0	0.029	2.616	0	0.027
10	0.028	2.614	10.32	0.027
20	0.028	2.606	20.63	0.026
30	0.026	2.594	30.92	0.025
40	0.025	2.578	41.18	0.024
50	0.023	2.557	51.4	0.023
60	0.022	2.534	61.59	0.021
70	0.021	2.509	71.72	0.02
80	0.02	2.482	81.8	0.02
90	0.02	2.454	91.83	0.02
100	0.02	2.427	101.8	0.02
110	0.02	2.401	111.72	0.021
120	0.021	2.377	121.59	0.022
130	0.022	2.356	131.4	0.023
140	0.023	2.337	141.18	0.024

Appendix C

Neutron detection data tables for two different detectors (e.g. ^3He and BF_3 gas filled detectors) [Fra99].

Data for BF_3 detector

Voltage	Number of counts
0	0
50	0
100	0
150	0
200	0
250	0
300	0
350	0
400	0
450	0
500	0
550	0
600	0
650	1
700	1
750	1
800	1
850	0
900	4
950	10
1000	59
1050	484
1100	699
1150	747
1200	801
1250	827
1300	809
1350	839
1400	842
1450	540
1500	812
1550	898
1600	889
1650	885
1700	857
1750	877
1800	969
1850	945
1900	1004
1950	943
2000	708

Data for LND ^3He detector

Voltage	Number of counts
800	0
850	2
900	68
950	141
1000	273
1050	426
1100	487
1150	520
1200	593
1250	679
1300	742
1350	748
1400	746

Appendix D

A number of successive readings from a radiation counter for repeated time intervals of equal length must be taken into consideration for the purpose of data characterization. Two elementary properties of the data must be considered, these are:

"Sum" $$\sum = \sum_{i=1}^{N} x_i \quad \text{... (D.1)}$$

"Experimental mean" $$\langle x_e \rangle = \sum / N \quad \text{... (D.2)}$$

It is also convenient to present data set by a corresponding frequency distribution function $F(X)$. The value of $F(X)$ is the relative frequency with which the number appears in the collection of data. By definition [Kno79]:

$$F(X) = \frac{X}{N} \quad \text{... (D.3)}$$

Where X and N are number of occurrences and measurements respectively. This parameter is very important because any set of data can be completely described by it frequency distribution function F(X). The distribution is automatically normalized that is,

$$\sum_{X=0}^{\infty} F(X) = 1 \quad \text{... (D.4)}$$

References:

[Adl85] R.J. Adler., *"Repetitively pulsed metal ion beams for ion implantation".* Nucl. Instr. and Meth. in Phy. Res. B 6, 123-128 (1985).

[And02] A. Anders., *"From plasma immersion ion implantation to deposition: a historical perspective on principles and trends".* Surf. Coat. Technol.vol. 156, 3-12 (2002).

[Bay04] B. Bayanov et al., *"Lithium neutron producing target for BINPaccelerator-based neutron source".* Applied Radiation Isotopes 61, 285-290 (2004).

[Bee06] F.C. De Beer., *"Personal communication"* (2006).

[Bie03] J.P. Biersack and J.F. Ziegler. Calculations using SRIM program.

[Cer04] J. Cerny et al., *"Study of neutron response and n-γ discrimination by charge comparison method for small liquid scintillation detector".* Nucl. Instr. and Meth. in Phys. Res. A 527, 512-518 (2004).

[Chu97] P.K. Chu and B.Y. Tang., *"Principles and characteristics of a new generation plasma immersion ion implanter".* Rev. Sci. Instrum. 68 (4), (1997).

[Cie82] S. Cierjacks., *"Neutron Physics and Data in Science and Technology".*vol 2. (Pergamon, New York) (1982).

[Col91] G.A. Collins, R. Hutchings and Tendys., *"Plasma immersion ion implantation of steels".* Material Science and Engineering. A 139, 171–178 (1991).

[Dar01] Darin Desilets and M. Zreda., *"On scaling nuclide production rate for altitude and latitude using cosmic-ray measurements"*. Earth and Planetary Letters 193, 213–225 (2001).

[Dav82] J.H. Dave et al.,*"The $^{1}H(^{7}Li,n)^{7}Be$ reaction as an intense MeV neutron source"*. Nucl. Instr. and Meth. 200, 285-290 (1982).

[Des06] S.S. Desai, A.M.Shaikh., *"On studies of ^{3}He and isobutene mixture as neutron proportional counter gas"*. Nucl. Instr. and Meth. in Phys. Res. A 557, 607-614 (2006).

[Ebe05] J.E. Eberhardt et al., *"Fast neutron radiography scanner for the detection of contraband in air cargo containers"*. Applied Radiation and Isotopes. 63, 179-188 (2005).

[Fra99] C.B. Franklyn., *"Use of proportional counters to detect neutrons experiment"*. (South Africa, NECSA) (1999).

[Fra06] C.B. Franklyn., *"Personal communication"* (2006).

[Hal38] O. Halpern, R. R. Lueneburg., *"On multiple scattering of neutrons"*. Phys. Rev. 53, 173 (1938).

[Hon05] Y.C. Hong., *"Generation of large-volume plasma by making use of multi-needle plasma at low-pressure"*. Thin solid Films 506 – 507, 474 – 478 (2005).

[htt01] http://www.chemcases.com/nuclear/nc-01.htm, taken on 2006/05/05.

[htt02] http://en.wikipedia.org/wiki/Neutron, taken on 2006/05/05.

[htt03] http://www.answers.com/neutrons, taken on 2006/01/19.

[htt04] http://hyperphysics.phy-astr.gsu.edu/HBASE?particles/parint.html#c4, taken on 2006/05/04.

[htt05] http://www.canberra.com/literature/936.asp, taken on 2006/02/22.

[htt06] http://www.particleadventure.org/frameless/npe.html, taken on 2007/02/21.

[Hub02] J. D. Huba., *"NRL plasma formular"*. Washington, DC 20375. (2002).

[Isb87] IAEA – ISBN 92-0-135087-2., *"handbook on nuclear activation data"*. Technical reports series No.273. (Vienna) (1987).

[Jas04] S.D. Jastaniah, P.J. Sellin., *"Digital techniques for n/γ pulse shape discrimination and capture-gated neutron spectroscopy using liquid scintillators"*. Nucl. Instr. and Meth. in Phys. Res. A 517, 202-210 (2004).

[Jef58] S. Jefferson., *"handbook of the atomic energy industry"*. (London) (1958).

[Kno79] G.F. Knoll., *"Radiation detectors and measurement"*. John Wiley and Sons, (New York) (1979).

[Kno00] G.F. Knoll., *"Radiation detector and measurements"*. Third edition, John Wiley and Sons, (New York) (2000).

[Kos79] G. Kostorz., *"Treatise on materials science and technology"*.vol 15. (New York) (1979).

[Lie89] M.A. Lieberman., *"Model of plasma immersion ion implantation"*. J.Appl, Phys.vol. 66, No. 7, (1989).

[Lin07] R. Lindsay., *"Personal communication"* (2006).

[Map04] K.P. Maphoto., *"Determination of Natural Radio activity Concentration in Soil: a comparative study of Windows and Full Spectrum Analysis"*. Department of Physics University of Western Cape Thesis, published thesis (2004).

[Mcg03] D.S. McGregor et al., *"Design considerations for thin film coated semiconductor thermal neutron detectors-I: basics regarding alpha particle emitting neutron reactive films"*. Nucl. Instr. and Meth. in Phys. Res. A 500, 272-308 (2003).

[Mit35] A.C.G. Mitchell, E.J. Murphy., *"Scattering of slow neutrons"*. Phys. Rev. 48, 653 (1935).

[Pro91] V.M. Prozesky., *"Proceedings of Surface Material Modification and Analysis Workshop"*. Energy Systems, (1991).

[Raw05] A. Rawazzani et al., *"Characterisation of ^{3}He proportional counters"*. Radiation Measurements. Received 9 March (2005); received in revised form 29 June 2005; accepted 23 August (2005).

[Rei05] J. Reijonen et al., *"D-D neutron generator development at LBNL"*. Applied Radiation and Isotopes. 63, 757-763 (2005).

[Rky06] R.K.Y. Fu et al., *"Ignition and dynamics of high-voltage glow discharge plasma implantation"*. Nucl. Instr. and Meth. in Phys. Res. B 242, 275 – 278 (2006).

[Rou03] J.J. Le Roux., *"Testing the durability of concrete with neutron radiography"*. Faculty of engineering University of Pretoria, unpublished thesis, (2003).

[Sas00] M. Sasaki et al., *"Feasibility studies of the self-TOF detector for high-energy neutron measurements in shielding experiment".* Nucl. Instr. and Meth. in Phys. Res. A 446, 545-554 (2000).

[Sch02] Michael Schneider and Matthew Thapson., *"New vacuum chamber for the plasma density transition-trapping experiment".* UCLA Department of Physics and Astronomy Los Angels, CA 90095. (2005).

[Ste91] R.A. Stewart and M.A. Lieberman., *"Model of plasma immersion ion implantation for voltage pulses with finite rise and fall times".* J. Appl. Phys. 70, 3480 (1991).

[Sxu06] S. Xu et al., *"Microstructure characteristics of steel M50 implanted with nitrogen by plasma-based ion implantation at elevated temperature".* Nucl. Instr. and Meth. in Phys. Res. B 242, 374 – 376 (2006).

[Tec00] IAEA – TECDOC – 1153: 2000., *"Use of accelerator based neutron sources".* IAEA (2000).

[Tec96] IAEA – TECDOC – 913: 1996., *"Manual for troubleshooting and upgrading of neutron generator".* IAEA (1996).

[Tes95] J.R. Tesmer, M. Nastasi (Eds)., "*Handbook of modern ion beam materials analysis",* Materials research society, Pittsburgh, P.A., (1995).

[Uhm91] Hans S. Uhm and W.M. Lee., *"High-dose neutron generation from plasma ion implantation".* J. Appl. Phys. 69, 8056 (1991).

[Wid70] M. Widner.,*"Ion Acoustic Wave Excitation and Ion sheath Evolution".* Phyics. Fluids.vol. 13, 2532 – 2540, (1970).

[Wol02] Wolhard Moller and Subroto Mukherjee., *"Plasma-based ion implantation".* Current Science.vol. 83, No. 3, (2002).

[www01] http://www.sciner.com /Neutron.Generation_Basic.htm, taken on 2006/01/18.

[www02] http:// www.plasmaengineering.com/ handbook. Htm, taken on 2006/02/16.

[www03] http//www.answers.com/main/ntq-s-neutron+detection, taken on 2006/02/21.

[Xiu99] Xiu Tian and Xiaofeng Wang., *"Special modular for high frequency, low-voltage plasma immersion ion implantation".* Rev. Sci. Instrum.vol. 70, No. 3, (1999).

[Zen03] P.D. Zencher et al., *"Neutron/γ-ray pulse-shape discriminator".* Nucl. Instr. and Meth. in Phys. Res. A 508, 434-439 (2003).

[Zie77] J.F. Ziegler and H.H. Andersen., *"Hydrogen stopping powers and ranges in all elements".* (Yorktown Heights, New York) (1977).